

# Heterotrimetallic Compounds Containing Mo-M-Li [M = K, Rb and Cs] Clusters: Synthesis, Structure, Bonding, Aromaticity and Theoretical Investigations of $\text{Li}_2\text{M}_2$ [M = K and Rb] and $\text{Cs}_4$ Rings

Dibakar Deb<sup>a</sup>, Soma Duley<sup>a</sup>, Slavko Radenković<sup>\*b</sup>, Patrick Bultinck<sup>c</sup>, Pratim K. Chattaraj<sup>\*a</sup> and Manish Bhattacharjee<sup>\*a</sup>

<sup>a</sup>*Department of Chemistry, Indian Institute of Technology, Kharagpur 721302, India*

<sup>b</sup>*Faculty of Science, University of Kragujevac, P. O. Box 60, 34000 Kragujevac, Serbia*

<sup>c</sup>*Department of Inorganic and Physical Chemistry, Ghent University, Krijgslaan 281 (S3), B-9000 Ghent, Belgium*

E-mail: [mxb@iitkgp.ac.in](mailto:mxb@iitkgp.ac.in),  
[pkc@chem.iitkgp.ernet.in](mailto:pkc@chem.iitkgp.ernet.in),  
[slavkoradenkovic@kg.ac.rs](mailto:slavkoradenkovic@kg.ac.rs)

## Abstract

A new polydentate fac-trioxo molybdenum complex,  $[\text{MoO}_3\text{L}]^{3-}$  { $\text{LH}_3$  = nitrilotriacetic acid} has been synthesized by the reaction of lithium molybdate and iminodiacetic acid. The trinegative complex anion coordinates the alkali metal cations,  $\text{K}^+$ ,  $\text{Rb}^+$  or  $\text{Cs}^+$ . The potassium, rubidium and cesium complexes,  $[\text{Li}\{\text{K}(\text{H}_2\text{O})_2\}\text{MoO}_3\text{L}]_n$  (1),  $[\text{Li}\{\text{Rb}(\text{H}_2\text{O})_2\}\text{MoO}_3\text{L}]_n$  (2) and  $[\text{Cs}\{\text{Li}(\text{H}_2\text{O})\}_2\text{MoO}_3\text{L}]_n$  (3), form heterotrimetallic coordination chains, containing planar rings of  $\text{Li}_2\text{M}_2$  (M = K or Rb) and  $\text{Cs}_4$ . Theoretical investigations on these rings were carried out using NICS calculations and ab initio ring current maps, revealing aromaticity to be of limited significance.

## 1. Introduction

Polymeric metal compounds have received a great deal of attention due to their properties, which lie between isolated molecules and bulk material.<sup>1-5</sup> Thus, a large number of metal organic framework materials<sup>6</sup>, metal oxide based materials<sup>7-9</sup> and metal clusters trapped within the channels of zeolites,<sup>10,11</sup> have been reported in recent years. These materials are important because of their possible application in catalysis,<sup>12,13</sup> gas storage,<sup>14-17</sup> electrical conductivity,<sup>18</sup> biology,<sup>19,20</sup> and many more areas. Molybdenum oxide based materials are interesting from a structural point of view<sup>21,22</sup> but molybdenum oxide based materials containing alkali metal clusters are rarely reported. Bimetallic compounds containing alkali metal clusters, for example gallium phosphonates, have been synthesized and shown to form cages containing lithium,<sup>1</sup> sodium, and potassium<sup>23</sup> ions with short metal-metal contacts.<sup>1</sup> These compounds are potential precursors for the preparation of ion conductors and molecular sieves.<sup>1</sup> This paper reports new molybdenum oxide based materials that share the characteristic short metal-metal interactions.

High-nuclearity heterometallic metal compounds are important from both a scientific and an industrial perspective because of their fascinating structures and interesting properties.<sup>23,24</sup> Their potential applications have drawn continuous attention in a number of research fields like chemistry,<sup>25-31</sup> biology,<sup>32,33</sup> physics,<sup>34-38</sup> and materials science.<sup>39-42</sup> Besides their structural appeal, these compounds can be used as functional materials with properties that are not derivable from either their homometallic analogues or their lower-nuclearity cognates. Moreover, such compounds are very difficult to synthesize. A great variety of cluster compounds have been reported in the literature, but reports on alkali metal clusters are rather few. In our previous work<sup>43-45</sup> the synthesis and structural characterization of  $[\text{Na}_2\text{MoO}_3\text{L}(\text{H}_2\text{O})_2]_n$ ,  $[\text{K}_2\text{MoO}_3\text{L}(\text{H}_2\text{O})_3]_n$ , and  $[\text{Li}_2\text{MoO}_3\text{L}(\text{H}_2\text{O})_2]_n$  (L=iminodiacetate) have been reported. The analysis of the crystal structures of those compounds showed that the Li- and Na-complexes contain linear chains of  $\text{Li}_6$  and  $\text{Na}_6$  hexagons, respectively, whereas the K-complex contains 2D hexagonal chains.

In the present paper we report the synthesis, characterization and structure of three heterotrimetallic compounds,  $[\text{Li}\{\text{K}(\text{H}_2\text{O})_2\}\text{MoO}_3\text{L}]_n$  (1),  $[\text{Li}\{\text{Rb}(\text{H}_2\text{O})_2\}\text{MoO}_3\text{L}]_n$  (2) and  $[\text{Cs}\{\text{Li}(\text{H}_2\text{O})\}_2\text{MoO}_3\text{L}]_n$  (3) { $\text{LH}_3$  = nitrilotriacetic acid}. These compounds contain molybdenum metalloligands and two different alkali metals besides a set of

rings composed entirely of metals. Besides the structural properties of the compounds, we therefore also studied the possible aromaticity/antiaromaticity in these rings. The cyclic systems  $\text{Li}_2\text{K}_2$  in **1**,  $\text{Li}_2\text{Rb}_2$  in **2** and  $\text{Cs}_4$  in **3** have been investigated and compared with the prototypical aromatic/antiaromatic benzene and cyclobutadiene. In order to assess the influence of Li atoms on their aromaticity/antiaromaticity two star-like Li derivatives, hexalithiobenzene and tetralithiocyclobutadiene<sup>46-48</sup> are included in the present discussion.

After the discovery of the aromatic character of  $[\text{Al}_4]^{2-}$  by Boldyrev *et al.*<sup>49,50</sup> the concept of aromaticity was extended from its usual organic realm to the field of all-metal inorganic clusters. In the recent past aromaticity of all-metal compounds gained a lot of attention.<sup>51-57</sup> In our previous work<sup>43-45</sup> the aromaticity of polyhexagonal Li-, Na- and K-clusters has been quantified by means of the nucleus-independent chemical shift (NICS).<sup>58</sup> It has been shown<sup>43-45</sup> that, according to NICS values, the aromaticity of hexagonal Li- and Na-clusters is of the same order of magnitude as the aromaticity of linear polyacenes, whereas the  $\text{K}_6$  rings are considerably less aromatic than the corresponding benzenoid systems.

In the present work the NICS, as one of the most popular aromaticity indices, has been used to gauge the aromaticity of the molecules considered. The problem with NICS, however, is that although usually a negative (or aromatic) NICS value reflects the existence of a ring current, there is no direct way to extract and thus beyond doubt prove the existence of an underlying ring current. There are several well-known examples<sup>59</sup> showing that NICS and ring current results do not agree. For this reason the obtained NICS results have been compared with current density maps calculated using the diamagnetic-zero variant of the continuous transformation of origin of current density (CTOCD-DZ) method.<sup>60-64</sup>

## 2. Experimental

Elemental analyses were performed using Perkin Elmer C, H, N, analyzer model 2400. The FTIR spectra were recorded on a Perkin Elmer FT-IR Spectrometer (SPECTRUM RXI). The  $^1\text{H}$  and  $^7\text{Li}$  NMR spectra are recorded on a Bruker AVANCE II ( $^1\text{H}$  frequency = 400 MHz) spectrometer. For  $^7\text{Li}$  spectra LiCl is used as external standard.

## X-ray crystallography

The single crystal data of the complexes **1**, **2** and **3** were collected on a Bruker APEX SMART CCD system that uses graphite monochromated Mo K $\alpha$  radiation ( $\lambda = 0.71073 \text{ \AA}$ ). The structure was solved by direct methods and refined by least square methods on  $F^2$  employing the WinGx<sup>65</sup> package and the relevant programs (SHELX-97<sup>66</sup> and ORTEP-3<sup>67</sup>) implemented therein. The hydrogen atoms on carbon and in water molecules were located in difference Fourier maps. The details of crystal data collection and refinement of **1**, **2** and **3** are summarized in Table 1. The important bond distances and bond angles are given in supplementary data (Table S2).

## Synthesis of Compounds, [Li{K(H<sub>2</sub>O)<sub>2</sub>}MoO<sub>3</sub>L]<sub>n</sub> (**1**) and [Li{Rb(H<sub>2</sub>O)<sub>2</sub>}MoO<sub>3</sub>L]<sub>n</sub> (**2**) and {LH<sub>3</sub> = nitrilotriacetic acid}

An aqueous solution of Li<sub>2</sub>MoO<sub>4</sub> (0.174g, 1 mmol) was added to an aqueous solution of nitrilotriacetic acid (0.191 g, 1 mmol) and the mixture was refluxed for about 6 hours. To the resulting solution was then added potassium chloride {0.149 g, 2 mmol). The mixture is then refluxed for 30 minutes. A few drops of an aqueous solution of LiOH·H<sub>2</sub>O were added to maintain the solution at pH ~ 4. The solution was filtered and the filtrate was allowed to stand in air at room temperature. Colorless plate-shaped crystals of **1**, suitable for X-ray diffraction, were obtained after one week. The same procedure was used for the synthesis of compounds **2** and **3**, using rubidium chloride {0.242 g, 2 mmol) and cesium chloride (0.338 g, 2 mmol), respectively, instead of potassium chloride. **1**: Yield; 81% (0.341 g). Elemental analysis calc (%) for C<sub>6</sub>H<sub>10</sub>Li<sub>2</sub>KMoNO<sub>11</sub> (421.066): C 17.12, H 2.39, N 3.30, found: C 17.41, H 2.28, N 3.42. IR (KBr) ( $\nu_{\max}$  /cm<sup>-1</sup>): 3309, 1620, 1403, 930, 900 and 870. <sup>1</sup>H NMR (D<sub>2</sub>O) (ppm): 3.85. <sup>7</sup>Li NMR (D<sub>2</sub>O) (ppm): 0.2 **2**: Yield: 74% (0.346 g). Elemental analysis calc (%) for **2** (C<sub>6</sub>H<sub>10</sub>Li<sub>2</sub>RbMoNO<sub>11</sub>) (Mw = 467.435): C 15.42, H 2.17, N 3.00; found: C 15.49, H 2.23, N 2.91. IR (KBr) ( $\nu_{\max}$  /cm<sup>-1</sup>): 3310, 1615, 1403, 930, 900, 860. <sup>1</sup>H NMR (D<sub>2</sub>O) (ppm): 3.83. <sup>7</sup>Li NMR (D<sub>2</sub>O) (ppm): 0.2. **3**: Yield: 78% (0.402 g). Elemental analysis calc (%) for **3** (C<sub>6</sub>H<sub>10</sub>Li<sub>2</sub>CsMoNO<sub>11</sub>) (Mw = 514.873): C 13.99, H 1.95, N 2.72; found: C 14.14, H 1.79, N 2.89. IR (KBr) ( $\nu_{\max}$  /cm<sup>-1</sup>): 3300, 1620, 1410, 910, 900, 850. <sup>1</sup>H NMR (D<sub>2</sub>O) (ppm): 3.78. <sup>7</sup>Li NMR (D<sub>2</sub>O) (ppm): 0.2.

### 3. Theoretical study

The structures of the  $\text{Li}_2\text{K}_2$ ,  $\text{Li}_2\text{Rb}_2$  and  $\text{Cs}_4$  rings were extracted from the experimental crystallographic data presented in this paper and studied without further geometry optimization to better reflect their characteristics as they appear in the complex. The molecular structures of the benzene, cyclobutadiene and star-like molecules  $\text{C}_4\text{Li}_4$  and  $\text{C}_6\text{Li}_6$  were optimized at the B3LYP/6-311+G(d,p) level. Computed Hessian matrices showed that all optimized structures correspond to minima on the potential energy surface.

NICS<sup>58</sup> values were calculated at B3LYP level through the gauge-including atomic orbital method (GIAO).<sup>68,69</sup> In these calculations the SDDALL basis set with the accompanying effective core potential was used, the same one used in the ring currents calculation.<sup>70-72</sup> There are several NICS indices in common use and since the NICS is a tensor, different components of the tensor are considered as appropriate indices of aromaticity. NICS calculated at the ring centre (NICS(0)) and 1 Å above the ring centre (NICS(1)) are among the most used NICS indices. Thus NICS(0) and NICS(1) have been used in this paper.

The current density maps presented in this paper were computed by means of coupled HF theory using the diamagnetic-zero variant of the continuous transformation of origin of current density (CTOCD-DZ) method.<sup>60-64</sup> In this method, the current density at each point in the molecule has been computed by choosing itself as the origin of the vector potential, hence the alternative name ‘ipsocentric’ for the method.<sup>73-75</sup>

**Table 1** Crystallographic data for **1** and **2**

Complex	<b>1</b>	<b>2</b>	<b>3</b>
Empirical formula	$\text{C}_6\text{H}_{10}\text{Li}_2\text{KMoNO}_{11}$	$\text{C}_6\text{H}_{10}\text{Li}_2\text{RbMoNO}_{11}$	$\text{C}_6\text{H}_{10}\text{Li}_2\text{CsMoNO}_{11}$
M (a.m.u)	421.066	467.435	514.873
Temperature, K	293(2)	293(2)	293(2)
Wavelength (Å)	0.71073	0.71073	0.71073
Crystal system	Monoclinic	Monoclinic	Monoclinic
Space group	$P2_1/c$	$P2_1/c$	$P2/c$

a (Å)	7.9807(10)	7.9395(4)	14.0195(13)
b (Å)	8.5886(11)	8.6813(4)	13.7541(13)
c (Å)	20.424(3)	20.6799(10)	7.7115(7)
$\beta$ (°)	96.724(4)	96.7070(10)	102.829(2)
V (Å <sup>3</sup> )	1390.3(3)	1415.61(12)	1449.9(2)
Z	4	4	2
D <sub>calc.</sub> (Mg/m <sup>3</sup> )	2.012	2.193	2.340
$\mu$ (Mo-K $\alpha$ ) (mm <sup>-1</sup> )	1.297	4.396	3.431
F(000)	832	904	960
$\theta$ Range (°)	2.01 to 26.46	1.98 to 31.18	1.48 to 31.37
Reflections collected	17378	20070	20606
Unique reflections/R(int)	2837/0.0699	4132/ 0.0336	4789/0.0259
Parameters/Restraints	216/0	240/0	229/0
Goodness of fit (F <sup>2</sup> )	1.055	1.018	1.063
R1	0.0331	0.0291	0.0320
wR2	0.0660	0.0611	0.0824

Current density maps for all molecules considered were also calculated using the SDDALL basis set including the effective core potential. It has been shown that by using basis sets with an effective core potential, one is able to reduce the impact of the core electrons thereby allowing a more efficient analysis of global current densities in Na-clusters.<sup>76</sup> In addition, NICS values calculated using an effective core potential are in good agreement with all electron NICS values.<sup>76</sup> In all calculations a unit magnetic field perpendicular to the molecular plane was used and the calculated ring currents were plotted on a grid in a set of planes parallel to the molecular plane with a diatropic current represented by a counterclockwise circulation.

The geometry optimization and calculation of NICS were performed by using Gaussian 03.<sup>77</sup> Calculations of ring currents were performed using our own Fortran routines requiring as input formatted checkpoint files from Gaussian 03.

## 4. Results and Discussion

Our synthetic strategy was to use a tetradentate, tribasic ligand ( $H_3L$ ), containing three carboxylate donor sites, which is expected to form the metalloligand,  $[MoO_3L]^{3-}$  at acidic pH (pH  $\sim$  4). The number of alkali metal ions required to neutralize the negative charge of the metalloligand anion was found to be higher than that reported for the metalloligands described in the earlier works from this laboratory.<sup>43-45</sup> We expected that, the tri- and tetra- negative metalloligands having multidentate donor sites (oxo ligands and carboxylate oxygens) have the potential to coordinate alkali-metal cations with interesting architecture.

### Synthesis and Characterization of **1**, **2** and **3**

Compound **1** has been synthesized by the reaction of nitrilotriacetic acid,  $Li_2MoO_4$  and potassium chloride in water. Compounds **2** and **3** have been prepared by the same procedure using rubidium chloride and cesium chloride, respectively, instead of potassium chloride. The compounds are colourless, highly crystalline and have been isolated in high yield. The compounds show low solubility in methanol and ethanol but are highly soluble in water and have been characterized by elemental analysis, IR and NMR spectroscopy as well as single crystal X-ray diffraction. The elemental analyses agree well with the compositions. The infrared spectra of the compounds exhibit strong bands at *ca.* 860, *ca.* 900 and at *ca.* 920  $cm^{-1}$  due to  $Mo=(O)_3$  stretching. In addition, a strong band appears at *ca.* 1620 and at *ca.* 1409  $cm^{-1}$  which are characteristic of coordinated  $-COO^-$  stretching frequencies. The broad band at around *ca.* 3300  $cm^{-1}$  can be assigned to the -OH stretching vibrations of the of water molecules.

The  $^1H$  ( $D_2O$ ) NMR spectra of the complexes in  $D_2O$  show a peak at *ca.* 3.80 ppm (singlet) due to the methylene protons. The  $^7Li$  NMR spectra of the complexes show a sharp singlet at *ca.* 0.2 ppm.

### Crystal Structure of $[Li\{K(H_2O)_2\}MoO_3L]_n$ (**1**) and $[Li\{Rb(H_2O)_2\}MoO_3L]_n$ (**2**)

One of the single crystals obtained by slow evaporation of the aqueous reaction solution was used for the determination of the solid-state structures by single crystal X-ray crystallography. X-ray diffraction analysis reveals that compounds **1** and **2** crystallize in the monoclinic space group  $P2_1/c$  and the compounds are isostructural. The asymmetric unit contains one molybdenum atom coordinated to a

nitrilotriacetate, one potassium/rubidium ion coordinated to two oxo ligands and carboxylate oxygen O4 and two lithium ions, coordinated to oxo oxygen O2 and carboxylate oxygen O9 in **1** and the carboxylate oxygens O5 and O9 in **2**. It is worth noting that there is a short-range interaction between the potassium and molybdenum ion in **1** (Fig. 1a) and the rubidium and molybdenum ion in **2** (Fig. 1b). Since the compounds are isostructural, the structural features of compound **1** have been described below.

The molybdenum center adopts a distorted octahedral geometry and is coordinated to three Mo=O oxygens, two carboxylate oxygens and the nitrogen of nitrilotriacetate. The three oxo oxygens (MoO<sub>3</sub>) are in a facial arrangement.

The metalloligand binds both potassium and lithium ions. Fig. 2 shows that each metalloligand binds three potassium ions through its carboxylate oxygens O4, O6 and O7, and the oxo oxygens O2 and O3. The metalloligand also binds six lithium ions through carboxylate oxygens O5, O7 and O9 and the oxo oxygens O1, O2 and O3. Oxygen atom O4 binds two potassium ions in a  $\mu_3$  fashion and O2 and O3 bind lithium and potassium ions in a  $\mu_3$  fashion. Oxygen atom O5 binds two lithium ions in a  $\mu_2$  fashion and O7 binds lithium and potassium ions in a  $\mu_2$  fashion. The most interesting feature of the structure is that each metalloligand binds the metal ions in such a way that a planar four member Li<sub>2</sub>K<sub>2</sub> unit is formed, where short Li-K interactions exist.

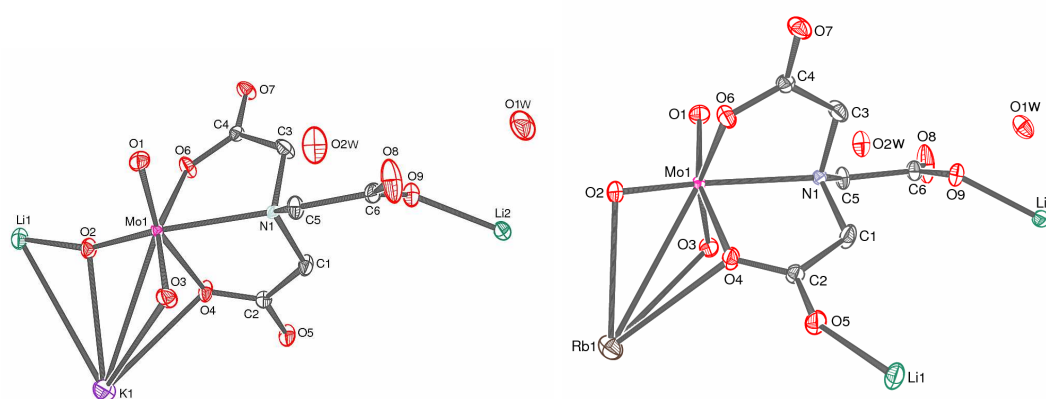


**Fig. 1** ORTEP view of the (a) Asymmetric unit of **1** and (b) Asymmetric unit of **2** with 30% thermal ellipsoid probability. Hydrogen atoms are not shown for clarity

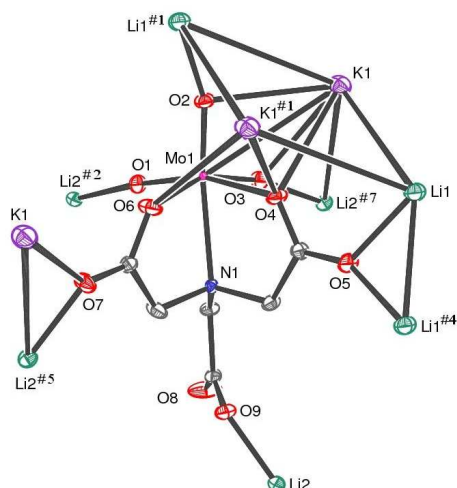


**Fig. 2** ORTEP view of the bonding mode of the metalloligand in **1**. Carbon atoms are not labeled

The K(1) ion is coordinated to oxo oxygens O2 and O3 and the carboxylate oxygen O4 of one metalloligand, carboxylate oxygens O4<sup>i</sup> ( $i = -x+1, -y+1, -z+1$ ) and O6 of a second metalloligand, and the carboxylate oxygen O7 of a third metalloligand and two water molecules, O1W and O2W. Thus, each K ion is bonded to three metalloligands (Fig. 3a). The oxygen atoms O2, O3 and O4 bridge both K1 and Mo1 in a  $\mu_3$  fashion. The observed Mo-K distance is 3.5737(10) Å. The short Mo-K distance clearly suggests the presence of a Mo...K interaction in the solid state.

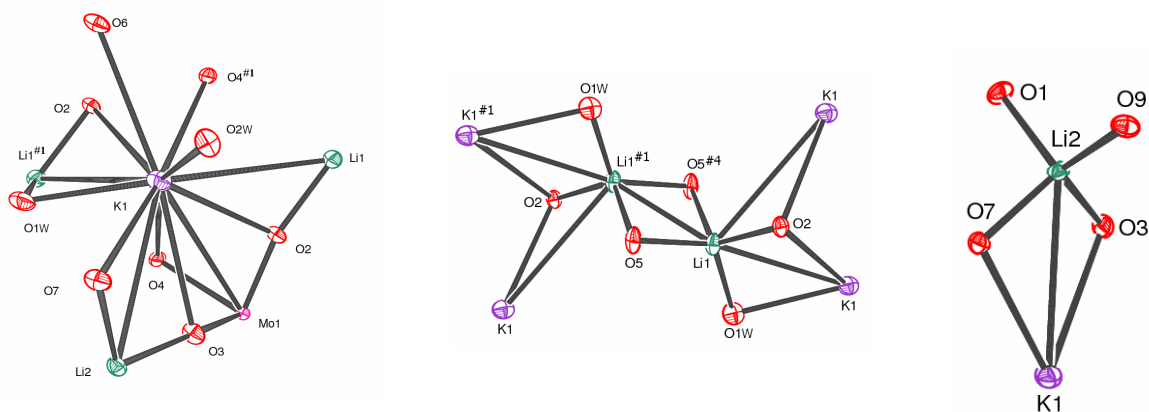


**Fig. 3** ORTEP view of the (a) Coordination environment of potassium ion. (b) & (c) Coordination environment of lithium ions

The coordination environments of the lithium ions are also noteworthy. Li1 is coordinated to oxo oxygen O2 from one metalloligand, two symmetrically equivalent

carboxylate oxygens: O5<sup>i</sup> and O5<sup>ii</sup> (ii = x+1, y, z) from two other metalloligands and water oxygen, O1W<sup>iii</sup> (iii = x+1, -y +3/2, z+1/2). Atoms O5<sup>i</sup> and O5<sup>ii</sup> bridge two lithium ions from opposite sides in a  $\mu_2$  fashion (Fig. 3b). Moreover, Li1 interacts with another Li1<sup>iii</sup> (iii = -x+2, -y+1, -z+1) with a distance of 2.7855(13) Å, which is distinctly shorter compared to elemental lithium (3.04 Å). Thus, each Li<sub>2</sub> (Li1-Li1<sup>iii</sup>) unit bridges four metalloligands. The coordination environment of Li2 is different from that of Li1. Lithium atom Li2 is coordinated to O1<sup>iv</sup> (iv = x-1, y, z), O3<sup>v</sup> (v = -x, y+1/2, -z+1/2), O7<sup>vi</sup> (vi = -x, y-1/2, -z+1/3) and O9 of four different metalloligands and in addition, it also shows an interaction with K1 (Fig. 3c). The observed Li2...K1 distance, {Li2–K1 = 3.624(6) Å} is rather short. Our literature survey did not reveal any reported crystal structure with such short Mo-K/Li-K interaction. Due to all the coordination, overall an infinite polymeric network is formed, extending along crystallographic *a*, *b* and *c* axis (Fig. 4a and 4b). In case of compound **2** similar types of Mo-Rb/Li-Rb interactions are observed in the solid state.

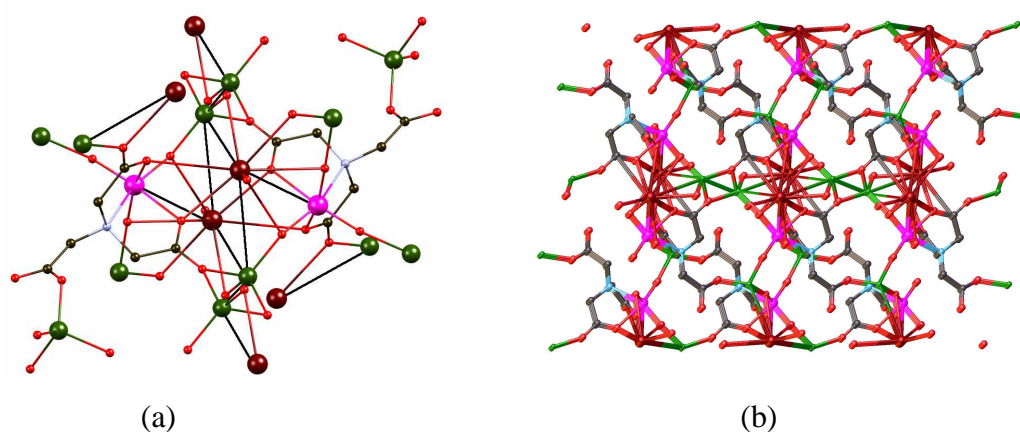


**Fig. 4** (a) Ball and stick model showing part of the polymeric structure. Metal-metal interactions are shown by black lines. (b) View along crystallographic *b* axis of the 3D network of **1**. Color Code: Mo: pink, Li: green, K: dark brown, O: red, N: light blue, C: black, H atoms are not shown for clarity.

The most interesting feature is the formation of the infinite heterotrimetallic metal cluster (Fig. 5). Due to the strong coordination of the potassium ion with two oxo oxygen atoms (O2, O3) and carboxylate oxygen O4 of one metalloligand, the two metal centers come very close to each other and as a result, establishing a Mo-K interaction in the solid state {Mo1- K1 = 3.5737(10) Å}. Another interesting feature of the structure is the formation of a planar four-member ring Li<sub>2</sub>K<sub>2</sub> {K1-Li1 =

3.852(7) Å and K1-Li1<sup>i</sup> = 3.579(7) Å}. The water oxygen O1W bridges Li and K in a  $\mu_2$  fashion and oxo oxygen O2 bridges Li and K in a  $\mu_3$  fashion, helping to stabilize this geometry. Another heterometallic interaction is observed between Li and K ions {Li2-K1 = 3.624(6) Å}. Finally, a homometallic interaction is observed between Li1 and Li1<sup>i</sup> {Li1-Li1<sup>i</sup> = 2.786(13) Å}. Overall an infinite heterotrimetallic cluster is formed in the polymeric structure which extends along the crystallographic *b* axis (Fig. 5a and 5c). Similar heterotrimetallic interactions and a planar four member ring formation are also observed in the solid state structure of **2** {Li1-Li1<sup>vii</sup> = 2.793(9) Å, Rb1<sup>vii</sup>-Li1 = 3.857(5) Å, Rb1-Li1<sup>vii</sup> = 3.695(5) Å, Rb1-Mo1 = 3.6687(4) Å (vii = -x + 1, -y + 1, z)} (Fig. 5b and 5c).

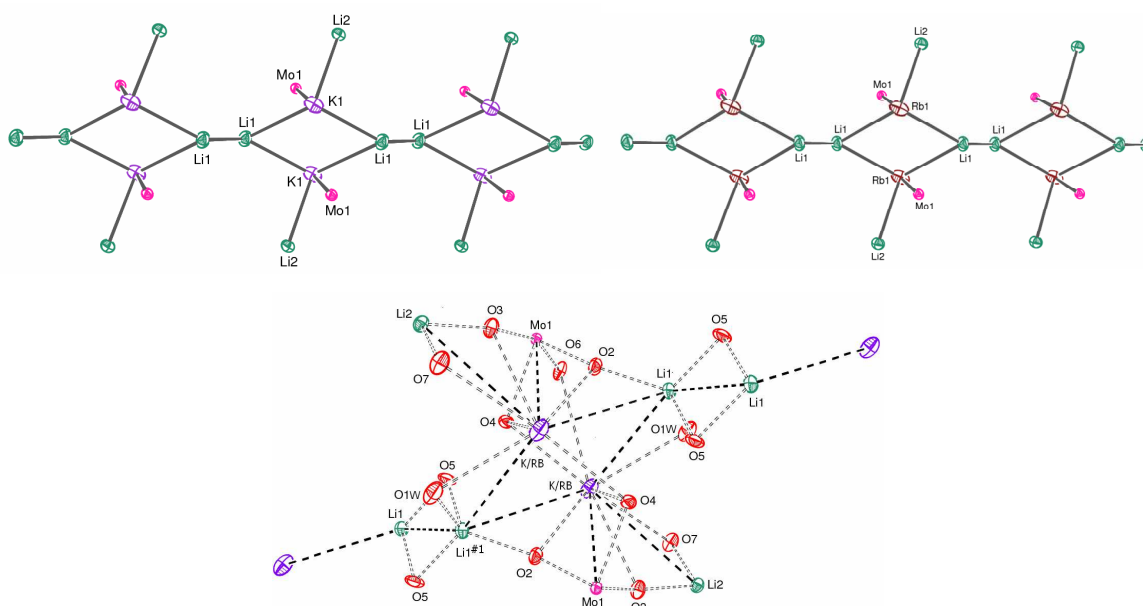


**Fig. 5** ORTEP view of (a) infinite heterotrimetallic metal cluster in **1(a)** and **2(b)**. (c) Stabilization of infinite heterotrimetallic metal cluster by bridging oxygens in complex **1/2**. Metal-metal interactions are shown by filled dashed lines

### Crystal Structure of [Cs(LiH<sub>2</sub>O)<sub>2</sub>MoO<sub>3</sub>L]<sub>n</sub> (**3**)

A suitable crystal for single crystal X-ray crystallography was obtained by slow evaporation of the reaction solution (water) at room temperature over a period of 10 to 15 days. The ORTEP view of the asymmetric unit of the complex is depicted in Fig. 6. Compound **3** crystallizes in the monoclinic space group *P2/c*. The asymmetric unit contains one molybdenum atom coordinated to a nitrilotriacetate and three -oxo

ligands. In addition it contains one cesium ion coordinated to two oxo ligands, four lithium ions, each with half occupancy, two water molecules coordinated to Li1 and Li4, and Li2 and Li3 coordinated to carboxylate oxygens, O8 and O9, respectively. Short solid-state interactions are observed between molybdenum and cesium on the one hand and cesium and lithium on the other. The molybdenum center adopts a distorted octahedral geometry.

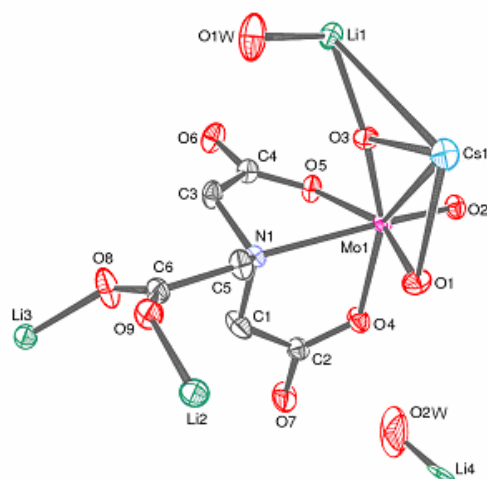


**Fig. 6** ORTEP view of the asymmetric unit of **3** with 30% thermal ellipsoid probability. Hydrogen atoms are not shown for clarity.

The metalloligand binds both cesium and lithium ions. Each metalloligand binds four cesium ions through its carboxylate oxygens O4 and O5, and three oxo oxygens, O1, O2, and O3 and also binds four lithium ions through carboxylate oxygens O7, O8, O9 and oxo oxygen atoms O3. Oxygen atom O1 binds two cesium ions in a  $\mu_3$  fashion and O2 binds three cesium ions in a  $\mu_4$  fashion. Oxygen atom O3 binds one lithium ion and two cesium ions in a  $\mu_4$  fashion and O9 binds two lithium ions in a  $\mu_2$  fashion. Here, the most interesting feature is the presence of metal-metal interactions. Each molybdenum ion interacts with four cesium ions and Li interacts with two cesium ions (Fig. 7a).

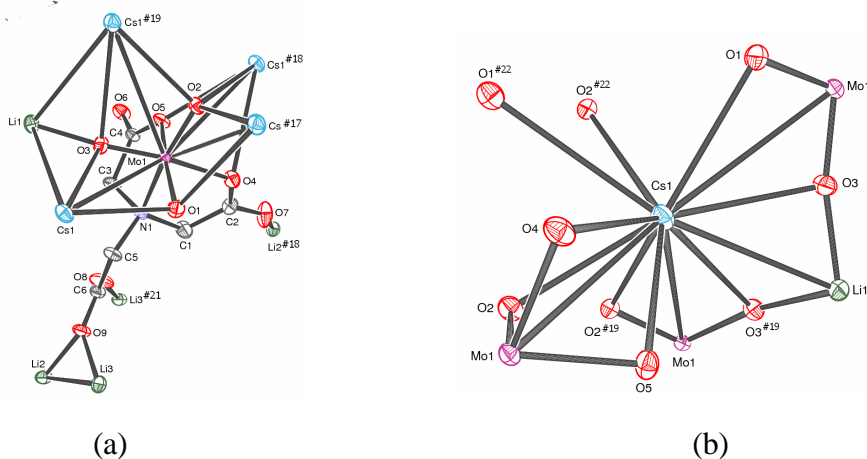


**Fig. 7** (a) ORTEP view of the bonding mode of the metalloligand in **3** (b) ORTEP view of the coordination environment of cesium ion. Hydrogen atoms are not shown for clarity.

In the compound, the cesium ion is coordinated to oxo oxygens O1 and O3 of one metalloligand, O1<sup>i</sup> ( $i = x, -y+1, z+1/2$ ) and O2<sup>i</sup> of another metalloligand, O2<sup>ii</sup>, O5<sup>ii</sup> and O4<sup>ii</sup> ( $ii = x, y, z+1$ ) of a third metalloligand and O2<sup>iii</sup> and O3<sup>iii</sup> ( $iii = -x, y, -z+3/2$ ) of a fourth metalloligand (Fig. 7b). Thus each cesium ion is coordinated to nine oxygens and is bonded to four metalloligands.

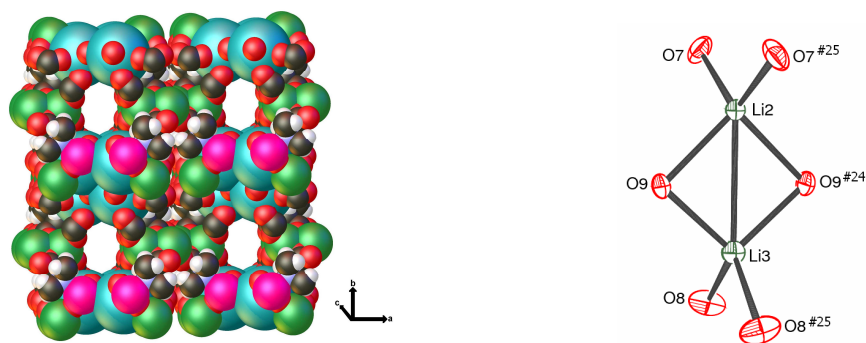


**Fig. 8** View of the infinite 3D porous anionic metal-organic frame work of **3** along the crystallographic  $c$  axis. Color Code: Mo: pink, Li: green, Cs: dark slate blue, O: red, N: light blue, C: black, H: white

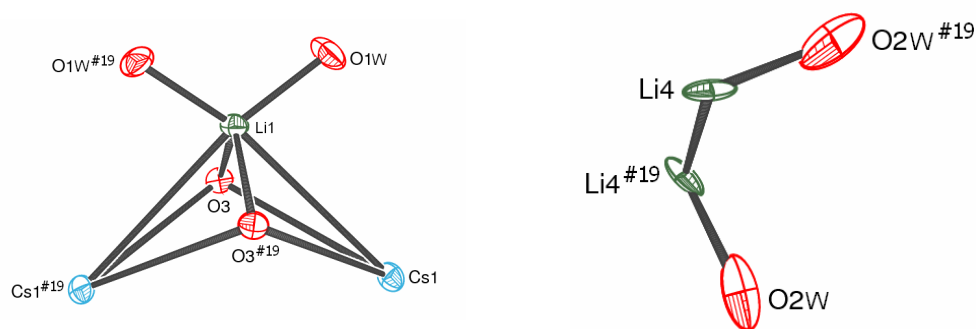


**Fig. 9** ORTEP view of the coordination environment of lithium ions in **3**

As a result, each cesium ion forms a node joining four metalloligands and in the solid an infinite 3D porous anionic metal-organic framework is formed which extends along crystallographic *a*, *b* and *c* axis. Loosely bound infinite chains of hydrated lithium ions,  $[\text{Li}_2(\text{H}_2\text{O})_2]^{2+}$  occupy the cavity formed (Fig. 8). The coordination environment of the lithium ions is also interesting (Fig. 9). Li1 is coordinated to two oxo oxygens O3 and O3<sup>iii</sup> from two metalloligands and also coordinated to two water oxygens, O1W and O1W<sup>iii</sup>. In addition Li1 lies in the vicinity of the two cesium ions Cs1 and Cs1<sup>iii</sup>. The most interesting feature is the formation of this heterometallic alkali metal cluster. The observed Li–Cs distance,  $\{\text{Li1–Cs1} = 3.648(6) \text{ \AA}\}$  is very short and suggests the presence of a Li...Cs interaction in solid state. Again, our literature survey did not reveal structures with such a short Li–Cs interaction. The coordination environment of Li2 and Li3 is the same. Both are in a tetrahedral coordination environment. Li2 is coordinated to two carboxylate oxygens: O7<sup>ii</sup>, O7<sup>v</sup> ( $v = -x+1, y, -z+3/2$ ) of two metalloligands and O9 and O9<sup>vi</sup> ( $vi = -x+1, y, -z+5/2$ ) of another two metalloligands. The lithium atom, Li3 is coordinated to O8 and O8<sup>vii</sup> ( $vii = -x+1, y, -z+3/2$ ) of two metalloligands and O9<sup>viii</sup> ( $viii = x, -y, z-1/2$ ) and O9<sup>ix</sup> ( $ix = -x+1, -y, -z+2$ ) of another two metalloligands. It is also observed that both lithium ions (Li2 and Li3) lie in each others proximity. The observed Li2–Li3 distance is 2.662(13) Å.

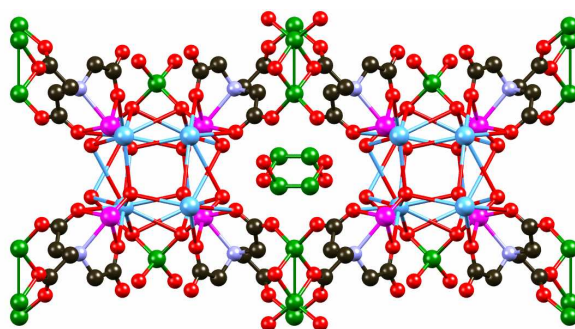


**Fig. 10** View along the crystallographic  $c$  axis of the 3D network of **3** containing 1D chain of lithium cluster,  $[\text{Li}_2(\text{H}_2\text{O})_2]^{2+}$  inside the cavity. Color Code: Mo: pink, Li: green, Cs: dark slate blue, O: red, N: light blue, C: black, H atoms are omitted for clarity.

Each metalloligand binds three  $\text{Li}_2$  ( $\text{Li}2\text{-Li}3$ ) units through its carboxylate oxygens O7, O8 and O9. Thus an infinite number of  $\text{Li}_2$  units are formed extending along the crystallographic  $c$  axis. Due to the presence of an infinite number of  $\text{Li}_2$  units and each  $\text{Li}_2$  unit joining six metalloligands, large channels extending along crystallographic  $c$  axis are created inside the crystal where an infinite number of water coordinated lithium ion clusters,  $[\text{Li}_2(\text{H}_2\text{O})_2]^{2+}$ , exist inside the cavity (Fig. 10). Inside the channel the lithium ion cluster,  $[\text{Li}_2(\text{H}_2\text{O})_2]^{2+}$  is loosely bound and is stabilized inside the cavity by the weak interaction of the atoms present inside the wall of the cavity with the lithium coordinated water molecules (Fig. 11a). Inside the cavity  $\text{Li}4$  coordinated water molecule, O2W is hydrogen bonded with carboxylate oxygen O8 of a metalloligand, and carboxylate oxygen O4 of a second metalloligand. Water oxygen O2W also interacts with another  $\text{Li}4$  of a nearer  $[\text{Li}_2(\text{H}_2\text{O})_2]^{2+}$  unit. Carboxylate oxygen O4 and oxo oxygen O1 of the second metalloligand also interact with ion  $\text{Li}4$ . Similar interactions are also observed in the case of the  $\text{Li}4$  ion. These interactions are responsible for stabilizing the  $[\text{Li}_2(\text{H}_2\text{O})_2]^{2+}$  ion inside the cavity. Due to the presence of interactions between  $\text{Li}$  coordinated water with the  $\text{Li}$  ions of successive  $[\text{Li}_2(\text{H}_2\text{O})_2]^{2+}$  units, an infinite 1D chain of  $[\text{Li}_2(\text{H}_2\text{O})_2]^{2+}$  units is stabilized inside the cavity. Another interesting feature of the chain is that all lithium ions in a cluster chain are in the same plane as evidenced by the observed torsion angle ( $\varphi$ ) of  $180^\circ$  between two adjacent lithium clusters. Similarly the observed torsion angle ( $\varphi$ ) between the water molecules coordinated to two adjacent clusters of lithium is also 180 degree (Fig. 11b). This geometry is also responsible for the formation and

stabilization of this cluster chain inside the cavity. The observed Li–Li distance {Li4–Li4 = 1.77(2) Å} is distinctly shorter compared to that in elemental lithium. It may be noted that the shortest Li...Li distances reported so far is 2.756 Å in the Li<sub>4</sub> chain in Li<sub>4</sub>[(MeGa)<sub>6</sub>(μ<sup>3</sup>-O)<sub>2</sub>(*t*-BuPO<sub>3</sub>)<sub>6</sub>](THF)<sub>4</sub>.<sup>1</sup> So this Li4-Li4 distance is the shortest distance till now reported in the literature.

Another interesting feature of the solid-state structure is the formation of a heterometallic infinite metal cluster. Among the three Mo=O oxygens, O1 bridges two cesium ions Cs1 and Cs1<sup>x</sup> (x = x, -y+1, z-1/2) in a μ<sup>3</sup> fashion and O2 bridges three cesium centers Cs1<sup>x</sup>, Cs1<sup>xi</sup> (xi = x, y, z-1) and Cs<sup>iii</sup> in a μ<sup>4</sup> fashion and O3 bridges cesium centers Cs1, Cs1<sup>iii</sup> and one Li ion in a μ<sup>4</sup> fashion. Thus, three oxo oxygen atoms from one metalloligand bridge with four cesium ions and one Li ion. The four observed Mo–Cs distances {Mo1–Cs1 = 3.9376(5) Å; Mo1–Cs1<sup>xi</sup> = 3.9610(5) Å; Mo1–Cs1<sup>iii</sup> = 3.9815(5) Å; Mo1–Cs1<sup>10</sup> = 4.0717(5) Å} are quite short and may be considered indicative of Mo...Cs interactions in the solid state. Other short solid-state interactions are observed between Cs and Li ions. Each lithium ion is in short contact with Cs1 and its symmetrically equivalent Cs1<sup>iii</sup> ion.

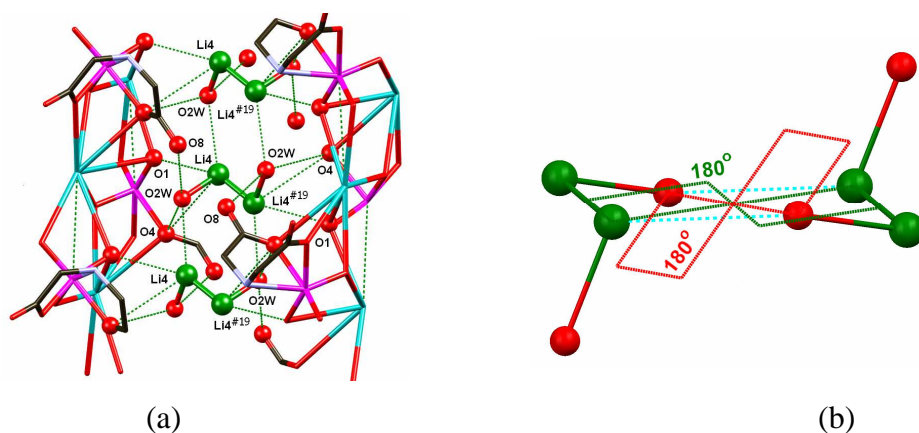


**Fig. 11** (a) Ball and stick model of the 1D chain of [Li<sub>2</sub>(H<sub>2</sub>O)<sub>2</sub>]<sup>2+</sup> ions present in the cavity. (b) Ball and stick model showing the exact geometry of two successive [Li<sub>2</sub>(H<sub>2</sub>O)<sub>2</sub>]<sup>2+</sup> ions present inside the cavity. Sky colored dotted lines shows the interaction between two successive [Li<sub>2</sub>(H<sub>2</sub>O)<sub>2</sub>]<sup>2+</sup> units. Color Code: Mo: pink; Li: green; Cs: dark slate blue; O: red; N: light blue; C: black. Hydrogen atoms and some portions of metalloligands have been omitted for clarity. Weak interactions are shown by green and light blue dotted lines.

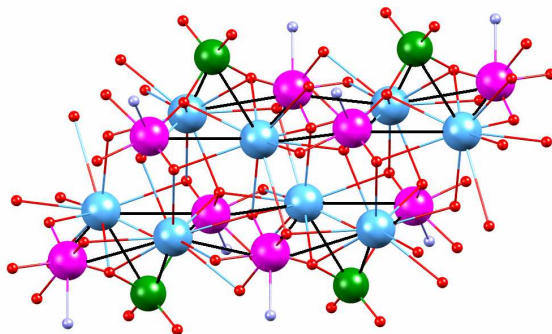


**Fig. 12** Ball and stick model of the part of polymeric structure showing the heterometallic metal-metal interactions by black lines. Color Code: Mo: pink, Li: green, Cs: dark slate blue, O: red, N: light blue.

The observed Li–Cs distance is 3.648(6) Å. It is important to note here that from a literature survey we did not find any report of the presence of Mo–Cs or Li–Cs short interactions in the solid state. Thus in the solid state an infinite heterotrimetallic cluster of Mo–Cs–Li is formed which extends along crystallographic *c* axis (Fig. 12).

### **Stability, Reactivity and Aromaticity**

Clearly, one of the most fascinating findings in the newly prepared compounds is the presence of unexpected all metal ring systems. The question on whether they are a significant contributor to the overall stability of these compounds or rather a consequence of the structure cannot be settled easily but based on the present interest in all metal aromaticity; an investigation of their stability is of contemporary interest. To that end, the geometries of the rings as found experimentally in the compounds and described above is extracted from the larger complexes and used for single point calculations of properties indicative of aromaticity. For these calculations, besides geometries, also the total charge must be known as well as the overall spin multiplicity. Given the importance of electrostatic interactions holding together many large solid-state structures, different total charges are considered and the evolution of the degree of aromaticity as a function of this charge is examined. For instance, in the case of  $Al_4$  rings, it is well-known that conclusions on the total aromaticity depend significantly on the total charge.<sup>78-81</sup> As spin multiplicity, in this report in all cases a singlet is assumed. This assumption is based on the fact that a geometry optimization

for the rings at the B3LYP/SDDALL level of theory led to a minimum energy geometry with only small or moderate changes in the geometry. At this geometry, the stability of the solution was checked, especially for the 4+ charge, and no other spin states were found with lower energy.

Conceptual DFT based reactivity descriptors are quite successful in analyzing the structure, stability, reactivity and the aromaticity of different systems<sup>82-84</sup> and include properties like the energy (E), electronegativity ( $\chi$ ), hardness ( $\eta$ ) and electrophilicity ( $\omega$ ). All have been computed at the same level of theory and are reported in Table 2.

Koopmans' approximation is used to calculate the required ionization potential and electronegativity. It may be noted that calculations using the neutral and the related charged species or a couple of calculations with fractional charges followed by the use of the corresponding frontier orbital energies a la Janak's theorem<sup>82</sup> would have produced better results. Replacement of K atoms by Rb atoms makes the system softer and more electrophilic. The planar Cs<sub>4</sub> ring is found to be the softest and the most electrophilic among all alkali systems studied. A likely reason may be the large size of the Cs atom. The aromaticity/antiaromaticity of all systems was scrutinized with the help of nucleus independent chemical shift (NICS) values. All the rings are planar in geometry and we performed the NICS calculations by placing the dummy atom at the geometrical center of the ring. The NICS values calculated at the B3LYP/SDDALL level for all molecules from Fig. 13 are given in Table 2. By inspection of the data in Table 2, it appears that the species containing four-membered rings are antiaromatic. According to NICS values both mixed rings Li<sub>2</sub>K<sub>2</sub> and Li<sub>2</sub>Rb<sub>2</sub> are somewhat less antiaromatic than the prototypical antiaromatic cyclobutadiene. On the other hand, the antiaromatic character of Cs<sub>4</sub> is even more pronounced than the antiaromatic character of cyclobutadiene. A notable feature of the calculated NICS values is that the presence of Li atoms in C<sub>6</sub>Li<sub>6</sub> results in a significant decrease of the aromatic character in these systems compared to benzene, and the antiaromaticity of C<sub>4</sub>Li<sub>4</sub> is more pronounced than the antiaromaticity of cyclobutadiene. Interestingly, the replacement of hydrogen atoms in benzene in cyclobutadiene by Li atoms results in much larger (i.e. more positive or less negative) NICS values, suggesting that alkaline metal ions may cause significantly anti-aromatic effects. The binding energy values for the corresponding ring systems are positive which implies that the bonding is energetically favorable.

**Table 2** Point group (PG), electronic state (ES), binding energy (BE, au), nucleus independent chemical shift [NICS(0) and NICS(1), ppm], electronegativity ( $\chi$ , eV), hardness ( $\eta$ , eV) and electrophilicity ( $\omega$ , eV) of the systems at B3LYP level with the SDDALL basis set. Calculations of conceptual DFT based global parameters are carried out using Koopmans' theorem.

Systems	PG	ES	BE	NICS(0)	NICS(1)	$\chi$	$\eta$	$\omega$
K <sub>2</sub> Li <sub>2</sub> -Ring	C <sub>2h</sub>	<sup>1</sup> A <sub>g</sub>	0.05247	10.00	9.08	2.233	1.069	2.333
Rb <sub>2</sub> Li <sub>2</sub> -Ring	C <sub>2h</sub>	<sup>1</sup> A <sub>g</sub>	0.04602	14.04	12.68	2.171	0.991	2.378
Cs <sub>4</sub> -Ring	C <sub>2h</sub>	<sup>1</sup> A <sub>g</sub>	0.02472	20.71	19.61	1.916	0.660	2.780
C <sub>4</sub> H <sub>4</sub> -Ring	D <sub>2h</sub>	<sup>1</sup> A <sub>1</sub>	1.48161	18.46	17.63	3.355	3.437	1.637
C <sub>4</sub> Li <sub>4</sub> -Ring	C <sub>2h</sub>	<sup>1</sup> A <sub>g</sub>	1.14749	36.18	22.59	1.886	2.144	0.829
C <sub>6</sub> H <sub>6</sub> -Ring	D <sub>6h</sub>	<sup>1</sup> A <sub>1g</sub>	2.46982	-12.65	-10.93	3.396	6.842	0.843
C <sub>6</sub> Li <sub>6</sub> -Ring	C <sub>6h</sub>	<sup>1</sup> A <sub>g</sub>	1.93138	4.47	-0.18	2.060	2.023	1.048

\*BE (Binding Energy) = Energy of isolated atoms - Total molecular energy

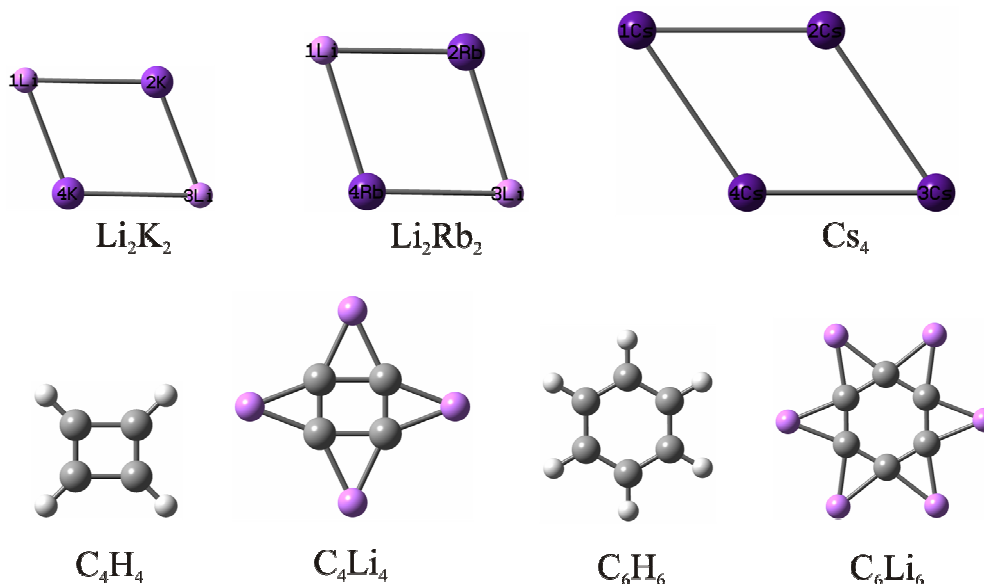


**Fig. 13** Structure of the molecules studied.

Complete NICS-scans for all molecules considered are presented in Fig. 14. It can be seen that in the case of Li<sub>2</sub>K<sub>2</sub>, Li<sub>2</sub>Rb<sub>2</sub> and Cs<sub>4</sub> NICS values become continuously smaller as one moves outwards from the ring plane. This is a typical feature of  $\sigma$ -

electron antiaromatic systems. On the other hand in the case of benzene, cyclobutadiene and  $C_6Li_6$  NICS-values have their extreme values at about 1 Å above the molecular plane due to effects of their frontier  $\pi$ -orbitals. It is interesting that for  $C_4Li_4$  NICS-values monotonically become smaller as one moves from the molecular plane, which indicates a predominant influence of the  $\sigma$ -electrons on its antiaromaticity. It should be noted that using NICS as an indicator of the aromaticity in  $C_6Li_6$  and  $C_4Li_4$ , systems with concentric rings can lead to some ambiguities. More detailed insight into aromaticity of such systems can be obtained using ring current maps.<sup>85</sup>

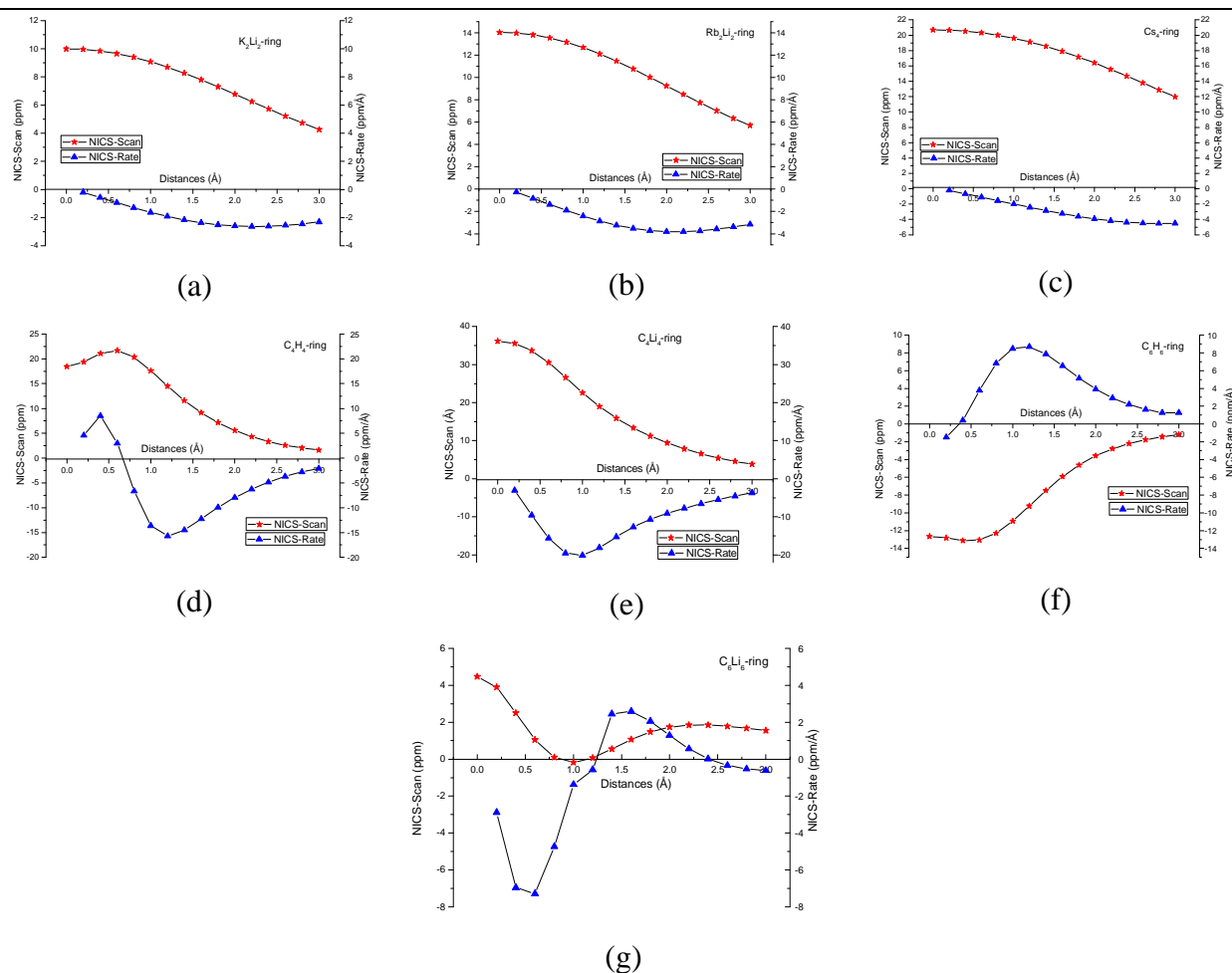


**Fig. 14** NICS-scans and NICS-rates for: a)  $Li_2K_2$  b)  $Li_2Rb_2$  c)  $Cs_4$  d) cyclobutadiene e)  $C_4Li_4$  f) benzene and g)  $C_6Li_6$ . NICS values are calculated at B3LYP level using the SDDALL basis set with the effective core potential.

The maps of the current density for  $Li_2K_2$ ,  $Li_2Rb_2$  and  $Cs_4$  calculated in the molecular plane are presented in Fig. (15-17). It should be noted that in all current density maps

of all alkali rings presented in this paper the arrow size is increased by a factor three compared to the arrow size used for current density maps of hydrocarbons and their Li derivatives. Although a basis set with an effective core potential is used in these calculations in order to reduce the impact of the core electrons, strong local currents around the K, Rb and Cs atoms are present in the ring current plots in Fig. (15-17). On the other hand, no such local circulations are found around the Li atoms (Fig. 15 and 16). This can be explained by the fact that the SDDALL pseudopotential is a small core pseudopotential for the K, Rb and Cs atoms, whereas only one active electron remains for Li. From Fig. (15-17) two characteristic features are immediately recognized. First,  $\text{Li}_2\text{K}_2$ ,  $\text{Li}_2\text{Rb}_2$  and  $\text{Cs}_4$  sustain a paratropic ring current. Second, the induced current density of these alkali systems is significantly weaker than in cyclobutadiene (Fig. 18a) and  $\text{C}_4\text{Li}_4$  (Fig. 19a). The last observation is in disagreement with the predictions made by NICS-values (Table 2). Fig. (15-17) also give current density maps for the orbitals that have individually significant contributions to the total current density. It can be seen that in  $\text{Li}_2\text{K}_2$ ,  $\text{Li}_2\text{Rb}_2$  and  $\text{Cs}_4$  almost all significant contributions come from the circulation of two  $\sigma$ -electrons from the HOMO. A somewhat different situation concerns  $\text{C}_6\text{Li}_6$  and  $\text{C}_4\text{Li}_4$  (Fig. 19). A distinguishing feature of these two systems is that due to presence of Li atoms their frontier HOMOs are  $\sigma$ -type orbitals. The doubly degenerate  $\sigma$ -HOMO in  $\text{C}_6\text{Li}_6$  and non-degenerate  $\sigma$ -HOMO in  $\text{C}_4\text{Li}_4$  have a significant paratropic contribution to the total current (Fig. 19b and 19e). The present orbital analysis shows that in  $\text{C}_6\text{Li}_6$  there are conflicting contributions, a paratropic (antiaromatic) from the doubly degenerate  $\sigma$ -HOMO and a diatropic (aromatic) from the degenerate  $\pi$ -HOMO-1. Such a possibility to manipulate the degree of aromaticity of benzene through replacing the hydrogen atoms on the benzene ring, is reminiscent of the case of hexa-iodobenzene where one can even further tune the aromaticity through changing the molecular charge.<sup>85</sup>

In the orbital analysis of the induced current density, the contribution of an occupied orbital is determined by the accessibility of the unoccupied orbitals by rotational and translational transitions.<sup>73</sup> The contribution of the given transition becomes more important as the energy difference between the occupied and virtual orbital is smaller. Rotational transitions lead to paratropic (antiaromatic) circulation, whereas translational transitions lead to diamagnetic (aromatic) circulation. For further

discussion it should be borne in mind that the similarity between the four-membered alkali rings and cyclobutadiene is clear although the symmetry of the compounds is not entirely the same. Details on the symmetry and electronic states of the molecules under investigation are given in Table 2. In the case of benzene the main contribution to the current density comes from translational transitions between the degenerate HOMO and LUMO levels (Fig. 20). In cyclobutadiene the most significant transition is the rotational transition: HOMO to LUMO, whereas all other transitions have less significant contributions as shown in Fig. 18b. The dominant transition in  $\text{Li}_2\text{K}_2$ ,  $\text{Li}_2\text{Rb}_2$  and  $\text{Cs}_4$  is the rotational transition between HOMO and LUMO, which is in complete analogy to cyclobutadiene. It should be noted that although the total current maps of benzene (Fig. 18c) and  $\text{C}_6\text{Li}_6$  (Fig. 19d) show that both systems sustain a diatropic ring current, the corresponding transition diagrams are quite different. In the case of  $\text{C}_6\text{Li}_6$  there is a strong rotational transition from the degenerate HOMO level to the doubly degenerate LUMO+2 level, but at the same time there is a somewhat weaker translational transition HOMO to the degenerate LUMO pair. As a result of these two transitions the contribution from the degenerate  $\sigma$ -HOMO pair is paratropic (Fig. 19e), but this contribution is still weaker than a diatropic contribution of the degenerate  $\pi$ -HOMO-1 pair. Similarly, in  $\text{C}_4\text{Li}_4$  compared to cyclobutadiene there is an additional rotational (antiaromatic) transition:  $\sigma$ -HOMO to LUMO.

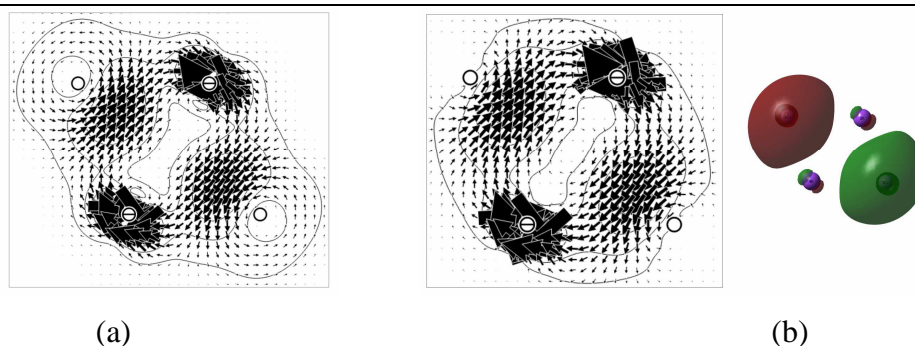
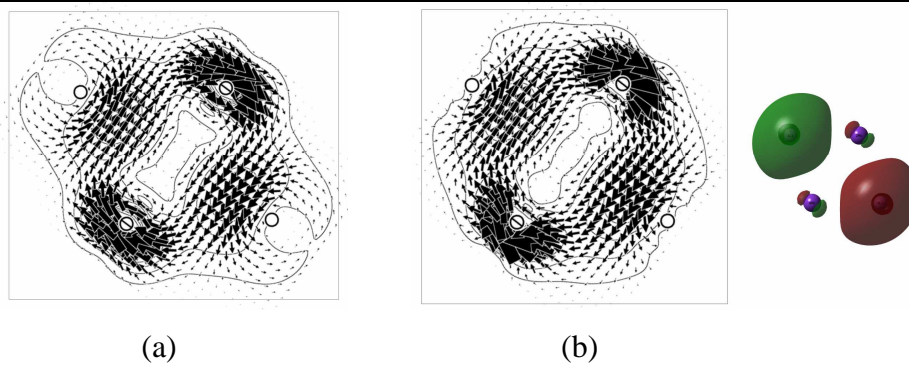
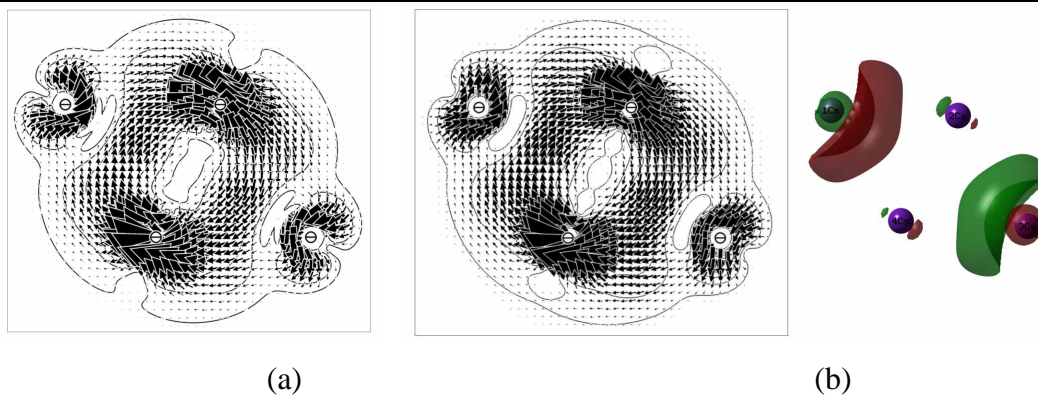


**Fig. 15** Current density maps of  $\text{Li}_2\text{K}_2$  in the molecular plane: a) total current density b) HOMO current density. Li and K atoms are represented by empty and bisected circles, respectively.



---

**Fig. 16** Current density maps of  $\text{Li}_2\text{Rb}_2$  in the molecular plane: a) total current density b) HOMO current density. Li and Rb atoms are represented by empty and bisected circles, respectively.



---

**Fig. 17** Current density maps of  $\text{Cs}_4$  in the molecular plane: a) total current density b) HOMO current density. Cs atoms are represented by bisected circles.

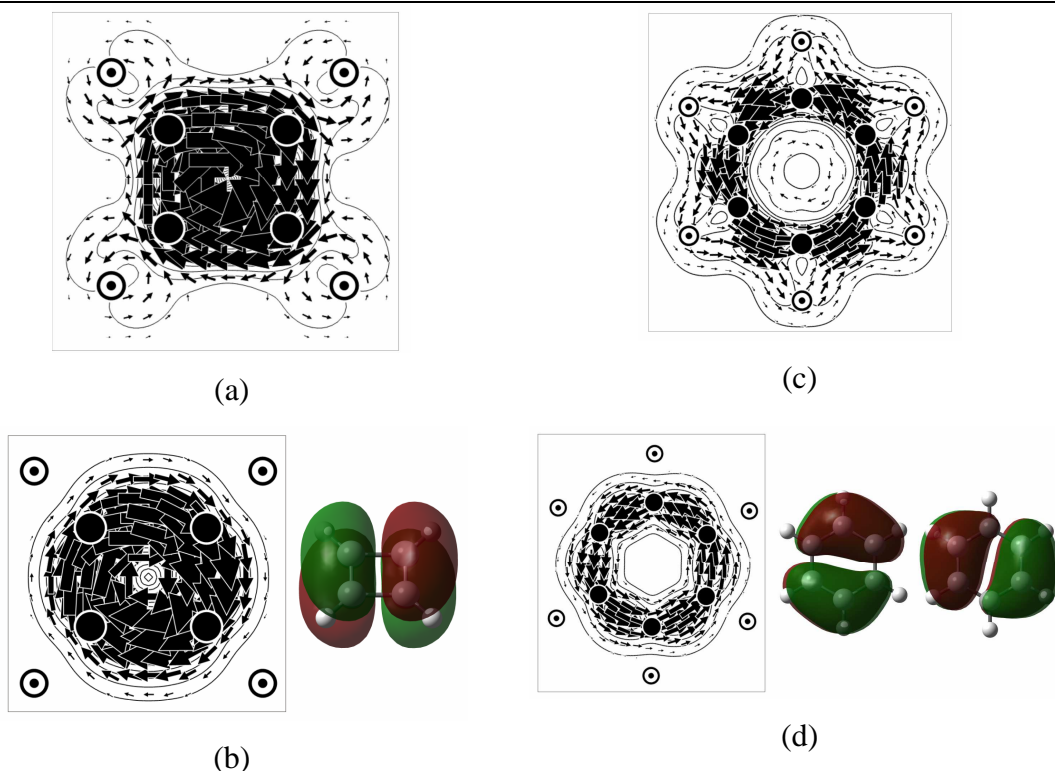


**Fig. 18** Current density maps of cyclobutadiene 1 Å above the molecular plane: a) total current density b) HOMO current density. Current density maps of benzene 1 Å above the molecular plane: c) total current density d) doubly degenerate HOMO current density. H and C atoms are represented by dotted and filled circles, respectively.

It is not trivial to extract quantitative information from current density plots. An indication of the current density strength is given by the largest magnitude of current density in the plotting plane. In the case of the alkali rings there are strong local currents around the alkali atoms. Therefore the largest magnitude of the current density in the plotting plane is not an appropriate indicator of the global current strength. It has been shown that the current bond cross sections and bond current strength can provide a very useful quantitative description of current density in the monocyclic molecules.<sup>86-88</sup> The largest magnitude of the bond current density cross sections ( $J_{max}$ ) can be taken as a measure of the global current density strength in the monocyclic systems. The largest magnitude of the bond current density cross sections for the molecules presented in Fig. 13 are given in Table 3. From these data (Table 3) it can be seen that the intensity of ring currents in  $\text{Li}_2\text{K}_2$ ,  $\text{Li}_2\text{Rb}_2$  and  $\text{Cs}_4$  is several

times smaller than the one in cyclobutadiene. This is completely opposite to the NICS values predicting the same order of magnitude of antiaromaticity of  $Cs_4$  and cyclobutadiene. The results from Table 3 show that  $\pi$ -electrons have about the same contributions in benzene and in its Li derivate  $C_6Li_6$  and in cyclobutadiene and  $C_4Li_4$ . Due to a paratropic contribution of frontier  $\sigma$  orbitals (Fig. 19e) the total current density in  $C_6Li_6$  is weaker than in benzene.

**Table 3** The largest magnitude of the bond total current cross sections ( $J_{\max}^{tot}$ ) and the largest magnitude of the bond  $\pi$ -electron current cross sections ( $J_{\max}^{\pi}$ ) expressed in a.u. The current density cross sections are calculated at the CTOCD-DZ/HF/SDDALL level.

System	bond	$J_{\max}^{tot}$	$J_{\max}^{\pi}$
$Li_2K_2$	Li1-K4	0.012	
$Li_2Rb_2$	Li1-Rb2	0.013	
$Cs_4$	Cs1-Cs2	0.016	
$C_4H_4$	C-C	0.158	0.097
$C_4Li_4$	C-C	0.147	0.098
$C_6H_6$	C-C	0.095	0.061
$C_6Li_6$	C-C	0.057	0.055

Table 3 also shows another interesting observation. In case of hydrocarbons like benzene and cyclobutadiene, there are clear ring currents going around the carbon atoms (see Fig. 18c for the typical case for benzene). In case of the all metal rings, the ring currents do certainly not envelope the metal atoms. This makes that it cannot be considered a true ring current on the same footing as the hydrocarbons. This is also clear from Table 3: the cross sections through the bonds have very small currents. This situation is quite different from ring current maps<sup>79,80,89</sup> for e.g.  $Al_4^{2-}$  where we do find a much more similar ring current map as in e.g., benzene. This suggests that on the one hand, the aromaticity of the all metal rings should be rather considered to be antiaromatici-*like* and that NICS cannot reflect the very detailed nature of the induced current, unlike the ring current maps.

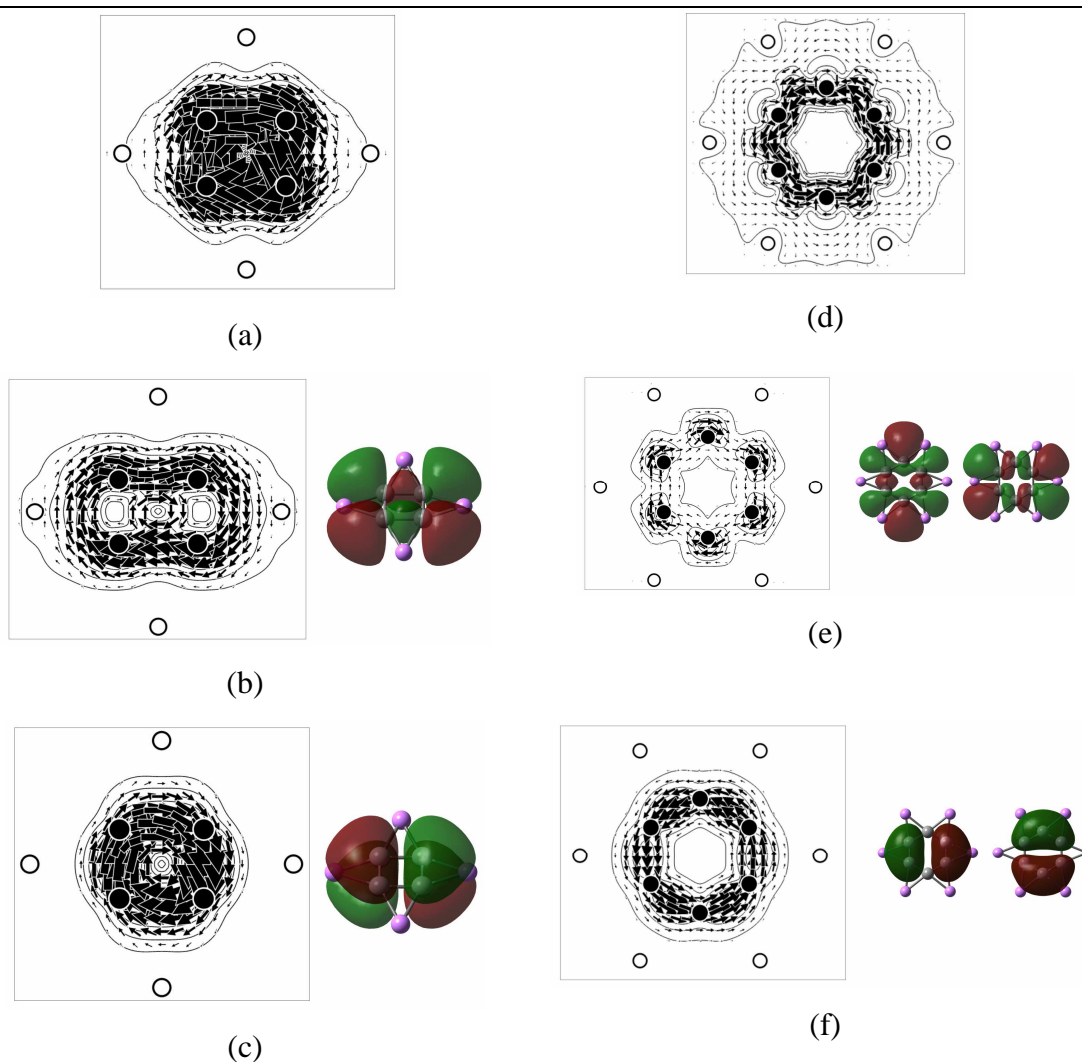


**Fig. 19** Current density maps of  $C_4Li_4$  1 Å above the molecular plane a) total current density b) HOMO current density c) HOMO-1 current density. Current density maps of  $C_6Li_6$  1 Å above the molecular plane: d) total current density e) degenerate HOMO pair current density f) degenerate HOMO-1 pair current density. Li and C atoms are represented by empty and filled circles, respectively.

All the above considerations were for neutral all metal rings. However, in the newly synthesized compounds, they may carry a relevant charge. Unfortunately, atomic charges are not observables and so depending on the population analysis used, different results may be obtained. Inspection of the transition diagrams giving rise to the ring current maps discussed above, leads to the suspicion that by changing the charge on the ring systems, one could tune the ring currents. This is indeed the case,

as is shown in Fig. 21. Fig. 22 presents the NICS scan and NICS rate plots for the  $K_2Li_2^{4+}$ ,  $Rb_2Li_2^{4+}$  and  $Cs_4^{4+}$ .

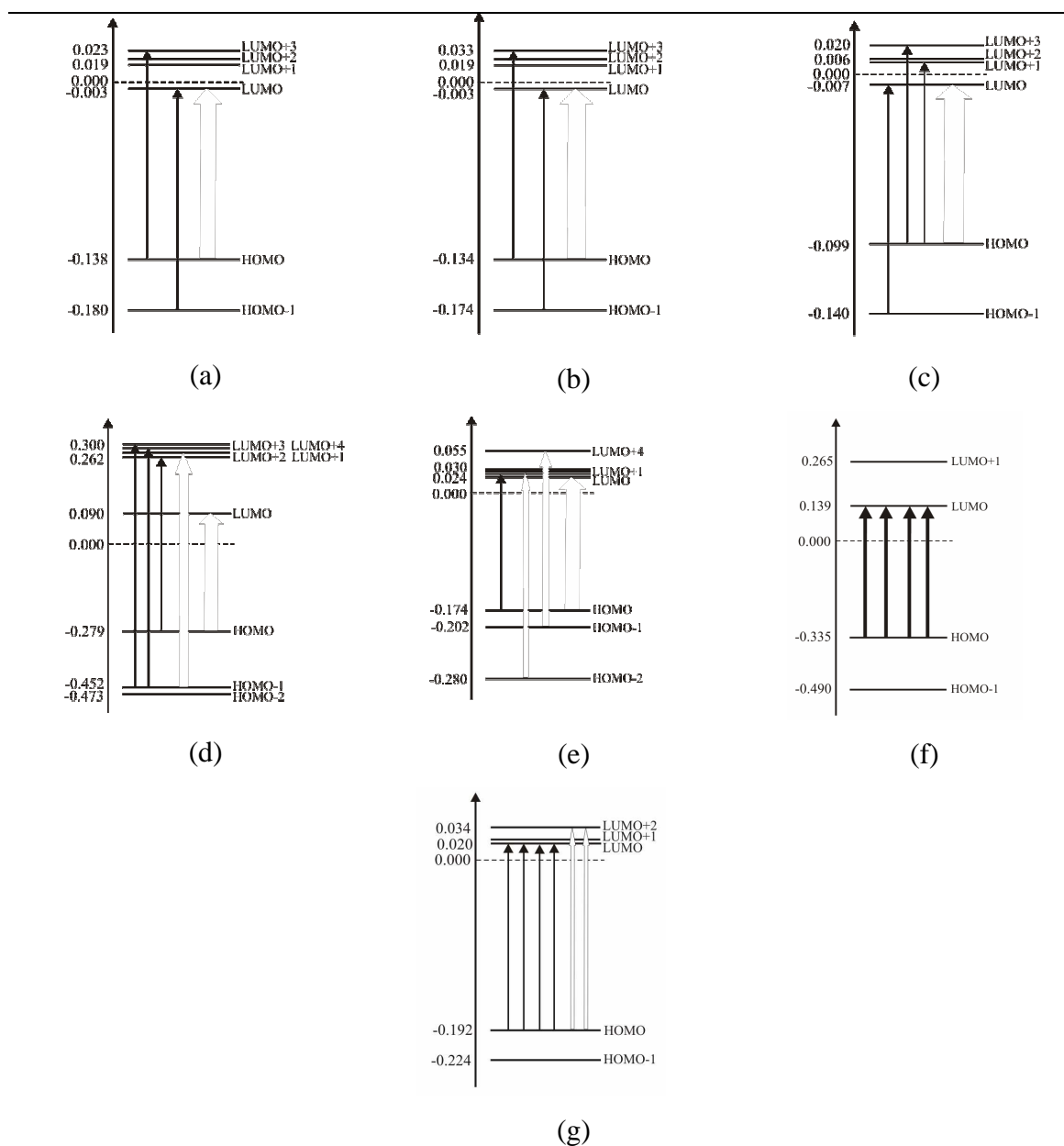


**Fig. 20** Orbital energy level diagram for: a)  $Li_2K_2$  b)  $Li_2Rb_2$  c)  $Cs_4$  d) cyclobutadiene e)  $C_4Li_4$  f) benzene and g)  $C_6Li_6$ . The energies (in a.u.) are obtained at the HF/SDDALL level. Only the transitions that significantly contribute to the induced current density are shown. Black arrows represent translational (diatropic) transitions and arrows without filling represent rotational (paratropic) transitions. The width of arrows reflects the relative magnitude of the contribution of the underlined transition (for details see Ref. 73).

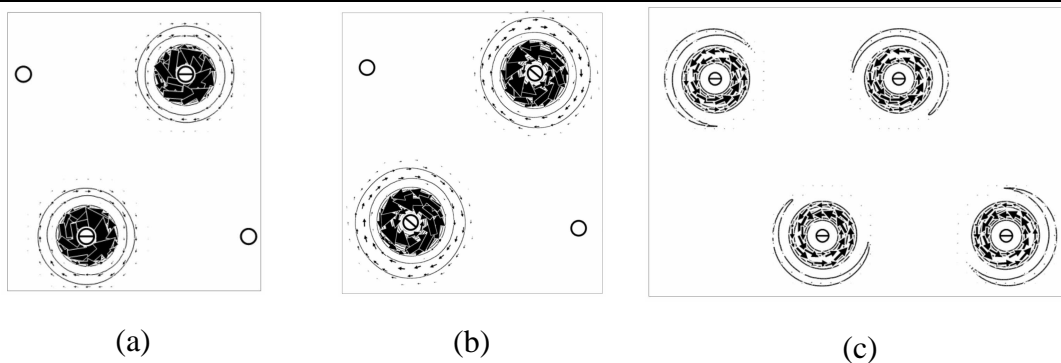


**Fig. 21** Current density maps in the molecular plane of a)  $\text{Li}_2\text{K}_2^{4+}$  b)  $\text{Li}_2\text{Rb}_2^{4+}$  and c)  $\text{Cs}_4^{4+}$ .

These findings very clearly show that in line with Fig. 20, the main contributors to the paratropic ring-current disappear because only occupied-virtual transitions are allowed and no significant contributions remain. NICS scans for these same compounds lead to the same conclusion. Given the fact that the ring currents, albeit significantly different from those in carbohydrates are already quite modest (and paratropic) in the neutral rings and disappear in the charged rings, plus the fact that the remaining part of the compound is likely to have a very significant impact on the electron features of the metallic rings, makes it very unlikely that in the compounds synthesized, aromaticity plays a significant role.

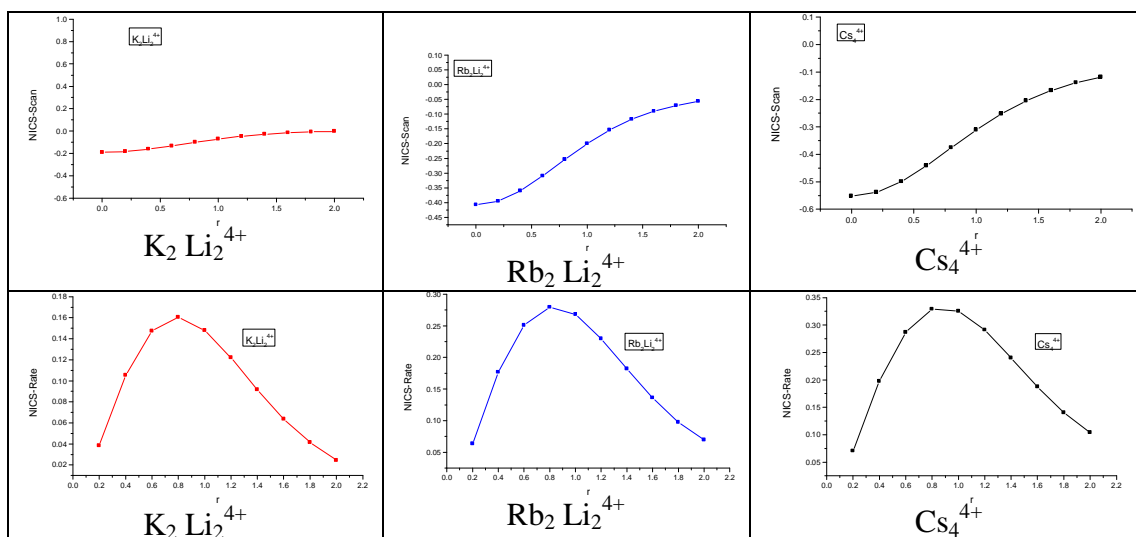


**Fig. 22** NICS scan and NICS rate plots for  $\text{K}_2\text{Li}_2^{4+}$ ,  $\text{Rb}_2\text{Li}_2^{4+}$  and  $\text{Cs}_4^{4+}$  rings at B3LYP/SDDALL level of theory.

## 5. Conclusions

A new polydentate *fac*-trioxo molybdenum metalloligand has been synthesized which binds group 1 metal cations,  $\text{Li}^+$  and  $\text{Rb}^+$ ,  $\text{K}^+$  and  $\text{Cs}^+$ . In solid state all the compounds form 3D heterotrimetallic coordination polymers. In compounds **1** and **2** a unique planar 1D chain of  $\text{Li}_2\text{M}_2$  ( $\text{M} = \text{K}$  or  $\text{Rb}$ ) rings is present. The compound **3** in solid state forms a 3D network containing cavities filled with chains of  $[\text{Li}_2(\text{H}_2\text{O})_2]$ . Analyses of the nucleus independent chemical shift data and the ring current plots reveal that most of the four membered rings exhibit paratropicity in their ring current albeit with a diminished strength for the all – metal rings compared to the most similar hydrocarbons. Moreover; the topology of the ring currents is so different compared to these hydrocarbons that the systems can hardly be described as truly aromatic or anti-aromatic. NICS, however, do not readily lead to this conclusion and ring current maps are needed to establish this. Finally, the ring current maps for ionic all metal rings were computed, showing that ring currents can be "switched on or off" depending on the total charge on the ring.

## Acknowledgement

DD and MB thank the Department of Science & Technology, Government of India, New Delhi for single crystal X-Ray and NMR facility and CSIR, New Delhi for financial assistance. SD thanks CSIR, New Delhi for financial support and PKC thanks DST, New Delhi for the J. C. Bose Fellowship. SR thanks the support by the Ministry of Science of Serbia, through Grant no. 174033. PB acknowledges the FWO-Vlaanderen for continuous support. Part of this work was carried out using the Stevin Supercomputer Infrastructure at Ghent University, funded by Ghent University, the Hercules Foundation and the Flemish Government – department EWI. We thank Mr. Sukanta Mondal for help in the manuscript preparation.

## References

1. M. G. Walawalkar, R. Murugavel, A. Voigt, H. W. Roesky, H. G. Schmidt, *J. Am. Chem. Soc.*, 1997, **119**, 4656-4661.
2. A. Schnepf, H. Schnöckel, *Angew. Chem. Int. Ed.*, 2002, **41**, 3532-3552.
3. D. K. Bohme, H. Schwarz, *Angew. Chem. Int. Ed.*, 2005, **44**, 2336-2354.
4. M. Pley, M. S. Wickleder, *Angew. Chem. Int. Ed.* 2004, **43**, 4168-4170.
5. J. W. Cheng, J. Zhang, S. T. Zheng, M. B. Zhang, G. Y. Yang, *Angew. Chem. Int. Ed.*, 2006, **45**, 73-77.
6. E. Burkholder, V. Golub, C. J. O'Connor, J. Zubieta, *Chem. Commun.* 2003, 2128-2129.
7. P. Hagrman, D. Hagrman, J. Zubieta, *Angew. Chem. Int. Ed.*, 1999, **38**, 2638-2684.
8. D. Hagrman, P. Hagrman, J. Zubieta, *Angew. Chem. Int. Ed.*, 1999, **38**, 3165-3168.
9. Q. Chen, J. Zubieta, *Coord. Chem. Rev.*, 1992, **114**, 107-167.
10. J. V. Casper, V. Ramamurthy, D. R. Corbin, *J. Am. Chem. Soc.*, 1991, **113**, 600-610.
11. P. P. Edwards, P. A. Anderson, J. M. Thomas, *Acc. Chem. Res.*, 1996, **29**, 23-29.
12. J. S. Seo, D. Whang, H. Lee, S. Jun, J. Oh, Y. J. Jeon, K. Kim, *Nature*, 2000, **404**, 982-986.
13. C.-D. Wu, A. Hu, L. Zhang, W. Lin, *J. Am. Chem. Soc.*, 2005, **127**, 8940-8941.
14. O. M. Yaghi, M. O'Keeffe, N. W. Ockwig, H. K. Chae, M. Eddaoudi, J. Kim, *Nature*, 2003, **423**, 705-714.
15. S. Kitagawa, R. Kitaura, S. Noro, *Angew. Chem. Int. Ed.*, 2004, **43**, 2334-2375.

16. K. S. Suslick, P. Bhyrappa, J.-H. Chou, M. E. Kosal, S. Nakagaki, D. W. Smithenry, S. R. Wilson, *Acc. Chem. Res.*, 2005, **38**, 283-291.
17. L. Pan, H. Liu, X. Lei, X. Huang, D. H. Olson, N. J. Turro, J. Li, *Angew. Chem. Int. Ed.*, 2003, **42**, 542-546.
18. C.-D. Wu, C.-Z. Lu, S.-F. Lu, H.-H. Zhuang, J.-S. Huang, *Dalton Trans.*, 2003, 3192-3198.
19. E. Rizzarelli, G. Vecchio, *Coord. Chem. Rev.*, 1999, **188**, 343-364.
20. J. S. Lindsey, *New J. Chem.*, 1991, **15**, 153-180.
21. E. Burkholder, V. Golub,; C. J. O'Connor, J. Zubieta, *Inorg. Chem.* 2003, **42**, 6729-6740.
22. Jr. R. S. Rarig, J. Zubieta, *J. Chem. Soc., Dalton Trans.*, 2001, 3446-3452.
23. A. Müller, *Science*, 2003, **300**, 749-750.
24. E. J. L. McInnes, S. Piligkos, G. A. Timco, R. E. P. Winpenny, *Coord. Chem. Rev.*, 2005, **249**, 2577-2590.
25. M. J. Moses, J. C. Fettinger, B. W. Eichhorn, *Science*, 2003, **300**, 778-781.
26. A. Dolbecq, E. Dumas, C. R. Mayer, P. Mialane, *Chem. Rev.*, 2010, **110**, 6009-6048.
27. C. I. Onet, L. Zhang, R. Clérac, J. B. Jean-Denis, M. Feeney, T. McCabe, W. Schmitt, *Inorg. Chem.*, 2011, **50**, 604-613.
28. A. Majumdar, K. Pal, K. Nagarajan, S. Sarkar, *Inorg. Chem.*, 2007, **46**, 6136-6147.
29. Y.-W. Li , Y.-G. Li, Y.-H. Wang, X.-J. Feng, Y. Lu, E.-B. Wang, *Inorg. Chem.*, 2009, **48**, 6452-6458.
30. R. Brusetti, O. Laborde, A. Sulpice, R. Calemczuk, M. Potel, P. Gougeon, *Phys. Rev. B*, 1995, **52**, 4481-4493.
31. Z. Zheng, *Chem. Commun.*, 2001, 2521-2529.

32. S. A. Bursakov, O. Y. Gavel, G. Di Rocco, J. Lampreia, J. Calvete, A. S. Pereira, J. J. Moura, I. Moura, *J. Inorg. Biochem.*, 2004, **98**, 833-840.
33. D. Coucouvanis, *Acc. Chem. Res.*, 1981, **14**, 201–209.
34. A. Mishra, W. Wernsdorfer, K. A. Abboud, G. Christou, *J. Am. Chem. Soc.*, 2004, **126**, 15648-15649.
35. V. M. Mereacre, M. Ako Ayuk; R. Clerac, W. Wernsdorfer, G. Filoti, J. Bartolome, C. E. Anson, A. K. Powell, *J. Am. Chem. Soc.*, 2007, **129**, 9248-9249.
36. L. M. C. Beltran, J. R. Long, *Acc. Chem. Res.*, 2005, **38**, 325-334.
37. M. Romanelli, G. A. Kumar, T. J. Emge, Richard E. Riman, J. G. Brennan, *Angew. Chem. Int. Ed. Engl.* 2008, **47**, 6049-6051.
38. C. M. Zaleski, E. C. Depperman, J. W. Kampf, M. L. Kirk, V. L. Pecoraro, *Angew. Chem. Int. Ed. Engl.*, 2004, **43**, 3912-3914.
39. T. Stamatatos, K. A. Abboud, W. Wernsdorfer, G. Christou, *Angew. Chem. Int. Ed. Engl.*, 2007, **46**, 884-888.
40. T. Liu, Y. Zhang, Z. Wang, S. Gao, *J. Am. Chem. Soc.*, 2008, **130**, 10500-10501.
41. S. Xiang, S. Hu, T. Sheng, R. Fu, X. Wu, X. Zhang, *J. Am. Chem. Soc.*, 2007, **129**, 15144-15146.
42. D. Gatteschi, R. Sessoli, *Angew. Chem. Int. Ed. Engl.*, 2003, **42**, 268-297.
43. S. Khatua, D. R. Roy, P. K. Chattaraj, M. Bhattacharjee, *Chem. Commun.*, 2007, 135-137.
44. S. Khatua, D. R. Roy, P. Bultinck, M. Bhattacharjee, P. K. Chattaraj, *Phys. Chem. Chem. Phys.*, 2008, **10**, 2461-2474.
45. D. Deb, S. Giri, P. K. Chattaraj, M. Bhattacharjee, *J. Phys. Chem. A*, 2010, **114**, 10871–10877.
46. J. R. Baran, R. J. Lagow, *J. Am. Chem. Soc.*, 1990, **112**, 9415 –9416.

47. E. D. Jemmis, G. Subramanian, A. J. Kos, P. v. R. Schleyer, *J. Am. Chem. Soc.* 1997, **119**, 9504–9512.
48. V. I. Minkin, R. M. Minyaev, A. G. Starikov, T. N. Gribanova, *Russ. J. Org. Chem.*, 2005, **41**, 1289–1295.
49. X. Li, A. E. Kuznetsov, H.-F. Zhang, A. I. Boldyrev, L.-S. Wang, *Science*, 2001, **291**, 859-861.
50. A. E. Kuznetsov, K. Birch, A. I. Boldyrev, X. Li, H. Zhai, L.-S. Wang, *Science*, 2003, **300**, 622-625.
51. A. I. Boldyrev, A. E. Kuznetsov, *Inorg. Chem.*, 2002, **41**, 532-537.
52. A. I. Boldyrev, L. –S. Wang, *Chem. Rev.*, 2005, **105**, 3716-3757.
53. C. A. Tsipis, *Coord. Chem. Rev.*, 2005, **249**, 2740-2762.
54. M. Mandado, A. Krishtal, C. Van Alsenoy, P. Bultinck, J. M. Hermida-Ramona, *J. Phys. Chem. A*, 2007, **111**, 11885-11893.
55. P. K. Chattaraj, D. R. Roy, M. Elango, V. Subramanian, *J. Phys. Chem. A*, 2005, **109**, 9590-9597.
56. P. K. Chattaraj, U. Sarkar, D. R. Roy, *J. Chem. Educ.*, 2007, **84**, 354-357.
57. D. Y. Zubarev, B. B. Avekiev, H. -J. Zhai, L. –S. Wang, A. I. Boldyrev, *Phys. Chem. Chem. Phys.*, 2008, **10**, 257-267.
58. P. v. R. Schleyer, C. Maerker, A. Dransfeld, H. Jiao, N. J. R. v. E. Hommes, *J. Am. Chem. Soc.*, 1996, **118**, 6317-6318.
59. R. W.A. Havenith, F. D. Proft, P. W. Fowler, P. Geerlings, *Chem. Phys. Lett.*, 2005, **407**, 391–396
60. T. A. Keith, R. F. W. Bader, *J. Chem. Phys.*, 1993, **99**, 3669-3682.
61. T. A. Keith, R. F. W. Bader, *W. Chem. Phys. Lett.*, 1993, **210**, 223-231.
62. S. Coriani, P. Lazzeretti, M. Malagoli, R. Zanasi, *Theor. Chim. Acta*, 1994, **89**, 181-192.

63. P. Lazzeretti, M. Malagoli, R. Zanasi, *Chem. Phys. Lett.* 1994, **220**, 299-304.
64. R. Zanasi, *J. Chem. Phys.*, 1996, **105**, 1460-1469.
65. L. J. Farrugia, *J. Appl. Crystallogr.*, 1999, **32**, 837-838.
66. G. M. Sheldrick, *Acta Crystallogr.*, 2008, **A64**, 112-122.
67. L. J. Farrugia, *J. Appl. Crystallogr.*, 1997, **30**, 565-666.
68. K. Wolinski, J. F. Hilton, P. Pulay, *J. Am. Chem. Soc.*, 1990, **112**, 8251-8260.
69. J. R. Cheeseman, G. W. Trucks, T. A. Keith, J. M. Frish, *J. Chem. Phys.*, 1996, **104**, 5497-5509.
70. A. Nicklass, M. Dolg, H. Stoll, H. Preuss, *J. Chem. Phys.* 1995, **102**, 8942-8952.
71. T. H., Jr. Dunning, P. J. Hay, *In Modern theoretical Chemistry*; H. F., Schaefer, III Ed.; Plenum: New York, 1976; Vol. 3; pp 1.
72. T. Leininger, A. Nicklass, H. Stoll, M. Dolg, P. Schwerdtfeger, *J. Chem. Phys.*, 1996, **105**, 1052-1059.
73. E. Steiner, P. W. Fowler, *J. Phys. Chem. A*, 2001, **105**, 9553-9562.
74. E. Steiner, P. W. Fowler, *Chem. Commun.*, 2001, 2220-2221.
75. P. W. Fowler, R. W. A. Havenith, *J. Phys. Chem. A*, 2002, **106**, 7048-7056.
76. Radenković, S.; Bultinck, P. *J. Phys Chem. A*, 2011, **115**, 12493–12502.
77. Gaussian 03, Revision C.02, M. J. Frisch, G. W. Trucks, H. B. Schlegel, G. E. Scuseria, M. A. Robb, J. R. Cheeseman, J. A. Jr. Montgomery, T. Vreven, K. N. Kudin, J. C. Burant, J. M. Millam, S. S. Iyengar, J. Tomasi, V. Barone, B. Mennucci, M. Cossi, G. Scalmani, N. Rega, G. A. Petersson, H. Nakatsuji, M. Hada, M. Ehara, K. Toyota, R. Fukuda, J. Hasegawa, M. Ishida, T. Nakajima, Y. Honda, O. Kitao, H. Nakai, M. Klene, X. Li, J. E. Knox, H. P. Hratchian, J. B. Cross, V. Bakken, C. Adamo, J. Jaramillo, R. Gomperts, R. E. Stratmann, O. Yazyev, A. J. Austin, R. Cammi, C. Pomelli, J. W. Ochterski, P. Y. Ayala, K. Morokuma, G. A. Voth, P. Salvador, J. J. Dannenberg, V. G. Zakrzewski, S. Dapprich, A. D. Daniels, M. C. Strain, O. Farkas, D. K. Malick, A. D.

- Rabuck, K. Raghavachari, J. B. Foresman, J. V. Ortiz, Q. Cui, A. G. Baboul, S. Clifford, J. Cioslowski, B. B. Stefanov, G. Liu, A. Liashenko, P. Piskorz, I. Komaromi, R. L. Martin, D. J. Fox, T. Keith, M. A. Al-Laham, C. Y. Peng, A. Nanayakkara, M. Challacombe, P. M. W. Gill, B. Johnson, W. Chen, M. W. Wong, C. Gonzalez, J. A. Pople, Gaussian, Inc., Wallingford CT, 2004.
78. (a) X. Li, A. E. Kuznetsov, H. -F. Zhang, A. I. Boldyrev, L. -S. Wang, *Science*, 2001, **291**, 859-861. (b) For antiaromaticity in  $\text{Li}_4$  see, A. N. Alexandrova, A. I. Boldyrev, *J. Phys. Chem. A*, 2003, **107**, 554-560.
79. P. W. Fowler, R. W. A. Havenith, E. Steiner, *Chem. Phys. Lett.*, 2001, **342**, 85-90. .
80. P. W. Fowler, R. W. A. Havenith, E. Steiner, *Chem. Phys. Lett.*, 2001, **359**, 530-536.
81. E. Steiner, P. W. Fowler, *Phys. Chem. Chem. Phys.*, 2006, **8**, 3383-3386.
82. R. G. Parr, W. Yang, *Density Functional Theory of Atoms and Molecules*; Oxford University Press: New York, 1989.
83. P. K. Chattaraj, *Chemical Reactivity Theory: A Density Functional View*; Taylor & Francis/CRC Press: Florida, 2009.
84. P. Geerlings, F. De Proft, W. Langenaeker, *Chem. Rev.*, 2003, **103**, 1793-1874.
85. R. W. A. Havenith, P. W. Fowler, F. Stijn, P. Bultinck, *Tetrahedron Lett.*, 2008, **49**, 1421-1424.
86. J. Jusélius, D. Sundholm, J. Gauss, *J. Chem. Phys.*, 2004, **121**, 3952-3963.
87. H. Fliegl, D. Sundholm, S. Taubert, J. Jusélius, W. Klopper, *J. Phys. Chem. A*, 2009, **113**, 8668-8676.
89. G. Monaco, R. Zanasi, S. Pelloni, P. Lazzeretti, *J. Chem. Theory Comput.*, 2010, **6**, 3343-3351.
90. P. Bultink, S. Fias, M. Mandado, R. Ponec, In "Aromaticity and Metal Clusters" P. K. Chattaraj (ed) Taylor & Francis, Florida, 2010 pp. 245-270.